

HyperGo: Probability-based Directed Hybrid Fuzzing

Peihong Lin
National University of Defense
Technology
Changsha, China
phlin22@nudt.edu.cn

Pengfei Wang
National University of Defense
Technology
Changsha, China
pawang@nudt.edu.cn

Xu Zhou
National University of Defense
Technology
Changsha, China
zhouxu@nudt.edu.cn

Wei Xie
National University of Defense
Technology
Changsha, China
xiewei@nudt.edu.cn

Kai Lu
National University of Defense
Technology
Changsha, China
kailu@nudt.edu.cn

Gen Zhang
National University of Defense
Technology
Changsha, China
zhanggen@nudt.edu.cn

ABSTRACT

Directed grey-box fuzzing (DGF) is a target-guided fuzzing intended for testing specific targets (e.g., the potential buggy code). Despite numerous techniques proposed to enhance directedness, the existing DGF techniques still face challenges, such as taking into account the difficulty of reaching different basic blocks when designing the fitness metric, and promoting the effectiveness of symbolic execution (SE) when solving the complex constraints in the path to the target. In this paper, we propose a directed hybrid fuzzer called HyperGo. To address the challenges, we introduce the concept of path probability and combine the probability with distance to form an adaptive fitness metric called *probability-based distance*. By combining the two factors, probability-based distance can adaptively guide DGF toward paths that are closer to the target and have more easy-to-satisfy path constraints. Then, we put forward an Optimized Symbolic Execution Complementary (OSEC) scheme to combine DGF and SE in a complementary manner. The OSEC would prune the unreachable branches and unsolvable branches, and prioritize symbolic execution of the seeds whose paths are closer to the target and have more branches that are difficult to be covered by DGF. We evaluated HyperGo on 2 benchmarks consisting of 21 programs with a total of 100 target sites. The experimental results show that HyperGo achieves 38.47×, 30.89×, 28.52×, 106.09× and 143.22× speedup compared to AFLGo, AFLGoSy, BEACON, WinDRanger, and ParmeSan, respectively in reaching target sites, and 3.44×, 3.63×, 4.10×, 3.26×, and 3.00× speedup in exposing known vulnerabilities. Moreover, HyperGo discovered 37 undisclosed vulnerabilities from 7 real-world programs.

CCS CONCEPTS

• Security and privacy → Software and application security.

Permission to make digital or hard copies of all or part of this work for personal or classroom use is granted without fee provided that copies are not made or distributed for profit or commercial advantage and that copies bear this notice and the full citation on the first page. Copyrights for components of this work owned by others than ACM must be honored. Abstracting with credit is permitted. To copy otherwise, or republish, to post on servers or to redistribute to lists, requires prior specific permission and/or a fee. Request permissions from permissions@acm.org.
CCS '23, November 26–30, 2023, Copenhagen, Denmark.

© 2023 Association for Computing Machinery.
ACM ISBN 978-x-xxxx-xxxx-x/YY/MM...\$15.00
<https://doi.org/10.1145/nnnnnnn.nnnnnnn>

KEYWORDS

Directed Greybox Fuzzing, Symbolic Execution, Hybrid Fuzzing, Software Security

ACM Reference Format:

Peihong Lin, Pengfei Wang, Xu Zhou, Wei Xie, Kai Lu, and Gen Zhang. 2023. HyperGo: Probability-based Directed Hybrid Fuzzing. In *Proceedings of the 2023 ACM SIGSAC Conference on Computer and Communications Security (CCS '23)*. ACM, New York, NY, USA, 16 pages. <https://doi.org/10.1145/nnnnnnn.nnnnnnn>

1 INTRODUCTION

Grey-box fuzzing has been a scalable and effective approach to discovering vulnerabilities in software in recent years [5, 6, 8, 11]. Based on the feedback information from the execution of the program under test (PUT), grey-box fuzzers utilize an evolutionary algorithm to generate specific inputs that can cause erroneous runtime behavior (e.g., memory corruptions or data abort) of PUT. Most existing fuzzers are coverage-guided (CGF) [10, 14, 20, 22] as they focus on improving the code coverage to test the deeper level of code. However, not all parts of the code in PUT are equally important because the majority of the code are safe and only a small portion has vulnerabilities. For example, according to Shin *et al.* [39], only 3% of the source code files in Mozilla Firefox have vulnerabilities. Thus, researchers aim to focus on strengthening the tests for the vulnerable parts of the code. To achieve directedness, the originally directed fuzzers were based on symbolic execution (SE) [15, 28, 29, 45], which uses program analysis and constraint solving to generate inputs that exercise different program paths. Such directed fuzzers cast the reachability problem as an iterative constraint satisfaction problem. However, since directed symbolic execution relies on heavyweight program analysis and constraint solving, it suffers from scalability and compatibility limitations [46].

In 2017, a directed grey-box fuzzer AFLGo [7] was proposed. It leverages lightweight compile-time instrumentation to drive the fuzzing toward a set of pre-defined target locations. Different from CGF which strives to increase the code coverage, DGF intends to reach and test the target sites (e.g., the potential buggy code). Based on the call graph and control-flow graph information of the PUT, DGF uses the distance between inputs and target sites as the fitness metric to assist seed selection and seed energy allocation. Thus, DGF can prioritize the seeds that are more likely to reach the targets

(i.e., optimal seeds), which makes DGF outperforms CGF in specific scenarios, such as patch testing [33], bug reproduction [17, 30, 43], and potential buggy code verification [40, 44]. To accelerate reaching targets and exposing vulnerabilities, the state-of-the-art DGF techniques proposed in recent years have employed various methods to enhance directedness. For instance, some DGF techniques redefine the fitness metric based on trace similarity (Hawkeye [9]), data-flow graph (CAFL [21], WindRanger [13]), and sequence coverage (LOLLY [26]) while some other DGF techniques prune infeasible paths (BEACON [16]), use the number of oracle queries required by a fuzzing algorithm to find a target-reaching input (MC^2 [38]) and utilize symbolic execution to penetrate the complex path constraints toward targets, namely directed hybrid fuzzing [12, 31, 32]. However, despite these achievements, the existing DGF techniques still face two challenges.

Challenge 1: Taking into account the difficulty of reaching different basic blocks to design a more effective fitness metric. Following AFLGo, most of the state-of-the-art DGF techniques proposed new fitness metrics and methods based on the knowledge of program analysis (e.g., DBB-distance in WindRanger and constraint-distance in CAFL). Although the methods can be beneficial in testing certain programs, they may be inaccurate while some specific programs do not meet their assumptions (e.g., WindRanger assumes that the complexity of path constraints is related to the number of corresponding seed bytes). During the fuzzing process, reaching different basic blocks have different probabilities since the path constraints are not all equally satisfied. It is challenging for the fuzzer to reach target sites through those basic blocks that are difficult to cover. Thus, it is a challenge to adaptively analyze the probability of reaching different basic blocks without prior knowledge of program analysis and combine the probability with the basic-block-level distance (i.e., BB distance) to form a more effective fitness metric.

Challenge 2: Promoting the effectiveness of symbolic execution when solving the complex constraints in the path to the targets. As DGF takes the random mutation, it may not be able to satisfy the complex constraints within the allotted time budget. To address this issue, a complementary symbolic execution technique can be introduced to assist DGF, which should meet three requirements: (1) preferentially solving the path constraints of the branches closer to target sites, (2) preferentially solving the path constraints of the branches that are difficult to be covered by DGF, and (3) pruning the branches that are unsolvable by symbolic execution or do not contribute to reaching the target. However, the symbolic execution techniques used in state-of-the-art hybrid fuzzers (such as SAVIOR [12], Symcc [36], DigFuzz [47], and Hyd-iff [32]) cannot meet all three requirements simultaneously. Thus, it is a challenge to design a complementary symbolic execution technique to effectively assist DGF.

In this paper, we propose HyperGo, the probability-based directed hybrid fuzzing. For challenge 1, we introduce the concept of path probability which is dynamically calculated based on branch hits, and then combine the path probability with BB distance to form an adaptive fitness metric called *probability-based distance*. The path probability reflects the difficulty of DGF reaching one basic block while the BB distance reflects the likelihood of DGF reaching

the target sites through the basic block. By combining the two factors, probability-based distance can effectively guide DGF toward paths that are closer to the target and have easier-to-satisfy path constraints (Section 3.1). Upon the introduction of a new fitness metric, it is imperative to optimize the power schedule to adaptively balance the exploitation of seeds with short distances and the exploration of more seeds that are reachable to the target sites (i.e., reachable seeds). To achieve this, we develop an optimization strategy for the power schedule called the Directed Multi-Armed Bandit (DMAB) model. Based on the continuously changing probability-based distance and path probability, the DMAB model adaptively assigns more energy to seeds that have shorter seed distances and higher probabilities of covering new branches.

For challenge 2, we propose an Optimal Symbolic Execution Complementary (i.e., OSEC) scheme that combines DGF and SE in a complementary way. In OSEC, we implement three strategies to improve the effectiveness of the combination between DGF and SE: (1) pruning branches that do not contribute to reaching target sites (i.e., unreachable branches), (2) pruning branches whose path constraints cannot be solved by SE (i.e., unsolvable branches), and (3) prioritizing the symbolic execution of the seeds whose paths are closer to the target and have more branches that are difficult to be covered by DGF. The first and second strategies aim at improving the efficiency of SE, while the third strategy aims at creating complementarity between SE and DGF. Specifically, we prompt DGF to explore branches with simpler path constraints, while SE is geared towards solving the path constraints of more complex branches. Based on this method, DGF and SE work in a complementary way and reach target sites more efficiently.

The main contributions of this paper are summarized as follows:

- We propose an adaptive fitness metric called probability-based distance, which combines basic-block-level distance with path probability to achieve higher accuracy and efficiency. It can steer DGF to reach the target sites faster through the closer paths which are easier to re-exercise.
- We propose a power scheduling optimization strategy called the DMAB model to implicitly balance the exploitation of seeds with short distances and the exploration of more reachable seeds. The seeds that have shorter seed distances and higher probabilities of covering new branches will be assigned more energy.
- We propose an OSEC scheme to combine DGF and SE in a complementary manner. The OSEC prunes the unreachable and unsolvable branches and prioritizes the symbolic execution of the seeds whose paths are closer to the target and have more branches that are difficult to be covered by DGF.
- We implemented a tool named HyperGo and evaluate it on 2 datasets consisting of 21 programs with a total of 100 target sites. The experimental results show that HyperGo achieves 38.47×, 30.89×, 28.52×, 106.09× and 143.22× speedup compared to AFLGo, AFLGoSy, BEACON, WindRanger, and ParmeSan, respectively in reaching target sites, and 3.44×, 3.63×, 4.10×, 3.26×, and 3.00× speedup in exposing known vulnerabilities. Moreover, HyperGo discovered 37 undisclosed vulnerabilities from 7 real-world programs.
- HyperGo is publicly available on our website. <https://gitee.com/paynelin/hypergo>

2 BACKGROUND AND MOTIVATION

2.1 Background

We first introduce the background knowledge of the DGF techniques and hybrid fuzzing techniques.

Distance calculation and power schedule. AFLGo calculates the distances between the inputs and predefined targets. The seed distance is calculated as the arithmetic mean of BB distances of the basic blocks in the seed's trace. The BB distance is determined by the number of edges in the call graph and control-flow graphs to the target basic blocks while each edge has the same weight. Then, at run-time, AFLGo views the fuzzing process as a Markov chain and leverages a simulated annealing strategy to gradually assign more energy to the seeds that are closer to targets. It casts reachability as an optimization problem to minimize the distance between the generated seeds and their targets.

Hybrid fuzzing. Hybrid fuzzing involves a combination of fuzzing and symbolic execution. Fuzzing is excellent at exploring common code regions and discovering more paths, while symbolic execution can track seed execution paths and reverse branch conditions to identify the branches that are not covered by fuzzing, namely *unexplored branches*. The constraint-solver is then invoked to solve the path constraints of the unexplored branches in the abstracted syntax and generate new seeds to assist fuzzing in satisfying the path constraints. However, existing hybrid fuzzing techniques are not well-suited to meet the needs of DGF, and they face four problems: (1) solving unreachable branches, (2) solving unsolvable branches, (3) solving the branches that had been covered by DGF, and (4) performing not well in adaptively adjusting the solving priority of seeds and the time budget of solving branches. These problems are more pronounced in DGF compared to CGF.

2.2 Motivation

Example of challenge 1. Figure 1 shows a real-world example (CVE-2017-15023) in GNU Binutils 2.29 [1]. Two execution traces (Trace 1 $\langle M, a, b, c, d, f \rangle$ is marked as red lines, and Trace 2 $\langle M, e, d, f \rangle$ is marked as blue lines) are toward the bug function `concat_filename()`. The call site of `concat_filename()` is denoted as T . Following AFLGo, the seed distance of the seed covering Trace 1 (i.e., Seed 1) should be $(1+2+3+4+3)/5=2.3$, and the seed distance of the seed covering Trace 2 (i.e., Seed 2) should be $(1+2+3)/3=2$. Thus, Seed 2 has a shorter seed distance and will be assigned more energy. WindRanger introduces the concept of *NumOfEffectiveBytes* and combines it with the seed distance to form a new fitness metric called *DBB-distance*. Based on the new fitness metric, Seed 1 still has a greater DBB-distance (2.18) than Seed 2's DBB-distance (2.06). Thus, in both works, Seed 2 is given priority.

However, since the path constraints in Trace 2 are stricter than those in Trace 1, it is more difficult for the fuzzer to satisfy the path constraints in Trace 2. For instance, the conditions leading to branch $\langle e, d \rangle$ ($if((unit \rightarrow line_table == NULL) \&\& (unit \rightarrow function_table == NULL))$) are harder for the fuzzer to penetrate through, resulting in that most of the executions will flow into the other branch $\langle e, h \rangle$. Therefore, even though Seed 2 is assigned more energy, its mutated inputs can hardly cover branch $\langle e, h \rangle$, making it unable to help DGF reach the target site. Based on this real-program-based example, **we can conclude that the static fitness**

metric based on program analysis may be inaccurate. We need an adaptive fitness metric that combines the probability to more accurately guide DGF in different real programs and different fuzzing stages.

Example of challenge 2. During our research, we investigated the state-of-the-art directed hybrid fuzzers and evaluated their performance in directed testing. For instance, we used SAVIOR [12] to test `tcpdump` five times, and each test lasted for 24 hours. According to the test results, we found that only 37% of them are reachable, only 28% of the attempts to generate new seeds are successful, and only 41% of the newly generated seeds are regarded as interesting. Furthermore, SAVIOR is incapable of dynamically adjusting the time budget for solving different branches, resulting in the skipping of some important branches within a very limited time budget and the inability to perform symbolic execution on all seeds within 24 hours. The investigation of SAVIOR demonstrates the issues of the state-of-the-art directed hybrid fuzzing techniques, such as solving unreachable or unsolvable branches, and generating a low proportion of interesting seeds. **Thus, we need to redesign the working scheme of symbolic execution to alleviate these issues and combine DGF and SE in a complementary manner.**

3 PROBABILITY-BASED DIRECTED HYBRID FUZZING

In this paper, we propose a probability-based directed hybrid fuzzer named HyperGo. As Figure 2 shows, HyperGo consists of the following three major components.

Static analyzer. The static analyzer is designed to provide precise information to both the directed greybox fuzzer and the symbolic executor, including unique basic block addresses, BB distances, and sibling branches of each branch. To calculate the address of all basic blocks, the static analyzer utilizes a hash algorithm based on the last statements of each basic block (for example, `exam.cpp:24` indicates line 24 of the file `exam.cpp`). Then, the static analyzer identifies sibling branches based on the successive basic blocks of each basic block. For example, if a basic block B_1 has two successors, B_2 and B_3 , the branch $\langle B_1, B_2 \rangle$ and branch $\langle B_1, B_3 \rangle$ are sibling branches. Additionally, we adopt the same method as AFLGo to calculate the BB distances.

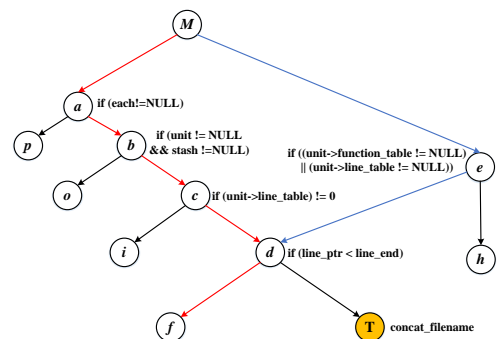


Figure 1: Two execution traces toward target function `concat_filename()`. The nodes denote the basic blocks, and the branch conditions are represented nearby.

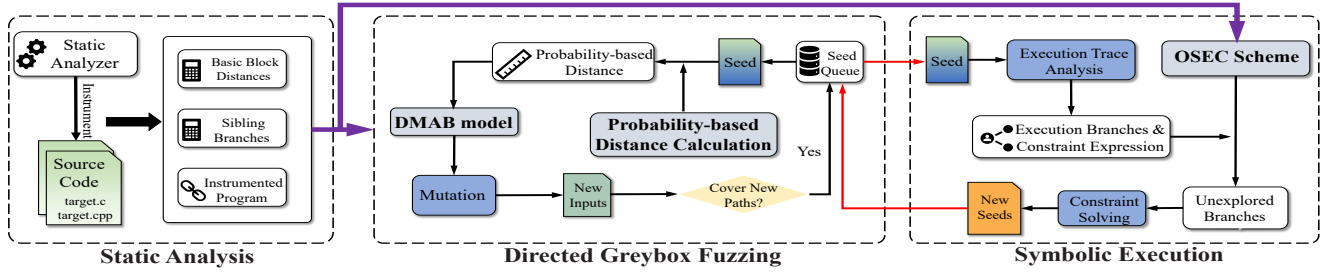


Figure 2: The overview of HyperGo.

Directed greybox fuzzer. The directed greybox fuzzer continuously mutates seeds in an attempt to generate inputs that can cover target sites. We introduce the probability-based distance calculation module and the DMAB model to the fuzzer. The calculation module calculates the probability-based distance by analyzing the statistical path probability and BB distance, and the DMAB model optimizes the power schedule based on this new fitness metric.

Symbolic executor. The symbolic executor tracks the path of the seeds provided by the directed greybox fuzzer to identify unexplored branches. It then invokes the constraint-solver to solve the path constraints of the unexplored branches and generate new inputs. We introduce the OSEC scheme to alleviate the limitations of hybrid fuzzing and complement the combination of DGF and SE.

At compile time, the static analyzer analyzes the program and stores the analysis information, such as BB distance, locally. This information is loaded by the directed greybox fuzzer and the symbolic executor as the fuzzing campaign is launched. During the fuzzing process, the directed greybox fuzzer continuously generates seeds and provides them to the symbolic executor. The symbolic executor tracks the paths of these seeds to identify unexplored branches and generates new inputs by solving path constraints of the unexplored branches. The new inputs are then fed back to the directed greybox fuzzer, enabling it to quickly reach target sites.

3.1 Probability-based Distance

We introduce the concept of path probability and combine it with BB distance to form an adaptive fitness metric called **probability-based distance**. In this section, we provide a detailed introduction to the concept and calculation method of probability-based distance.

3.1.1 Definition of Probability-based Distance. In recent works, such as MDPC [42], a seed's execution trace in fuzzing is treated as a Markov Chain, and the path probability is calculated based on branch probabilities in the execution path. Based on this assumption, we propose a definition for path and path probability:

Definition 1 (The path of a basic block) Given the execution trace *Trace* for a seed and a basic block *m* in *Trace*, the path of *m*, denoted as $path_m$, is a sequence of basic blocks in *Trace* from the entry basic block to *m*.

Definition 2 (Path Probability) The path probability of a basic block *m*, given its path $path_m$, is defined as the product of the probabilities of the branches that are covered by $path_m$:

$$P(path_m) = \prod \{P(br_i) | br_i \in path_m\} \quad (1)$$

Where br_i denotes a branch in $path_m$, $P(path_m)$ and $P(br_i)$ denote the path probability and branch probability, respectively. The branch probability is calculated based on the branch hits:

$$P(br_j) = \frac{hit_j}{\sum_{k=1}^{total} (hit_k)}, \quad (2)$$

Where $P(br_j)$ denotes the branch probability of the j^{th} branch of the branch condition (j can be 1 or 2 for a binary branch), *total* denotes the total number of branches, and hit_j denotes the number of branch hits of the j^{th} branch. Notably, the branch hits of the branches that are not covered by fuzzing will be regarded as 1 since we believe that any branch has the probability of being discovered.

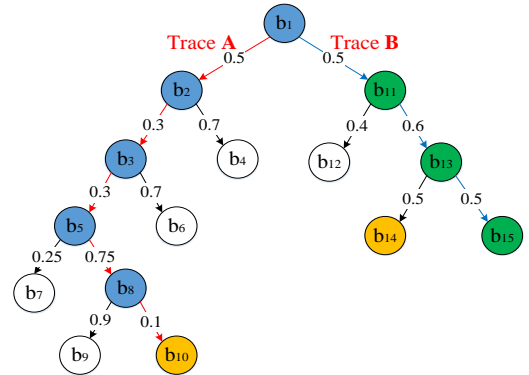


Figure 3: The calculating method of path probability.

Since the fuzzer utilizes a random mutation strategy, the process of fuzzing can be viewed as a form of random sampling. As the number of samples increases in random sampling, the statistical probability will gradually approach the theoretical probability. Therefore, it is reasonable to expect that the statistical branch probabilities and path probabilities will converge toward their theoretical values with the increasing number of mutations in fuzzing.

As shown in Figure 3, we use a simple artificial C program as an example to illustrate how we calculate branch probability and path probability. In Figure 3, each node (e.g., b_1) represents a basic block, and each edge (e.g., $\langle b_1, b_2 \rangle$) represents a basic block transition (i.e., branch). The path towards b_5 is a sequence of basic blocks starting from the entry basic block b_1 , represented as $\langle b_1, b_2, b_3, b_5 \rangle$. The digitals above the line (e.g., 0.5 above branch $\langle b_1, b_2 \rangle$) represent the branch probabilities evaluated based on statistical probabilities. For example, if the branch hits of $\langle b_1, b_2 \rangle$ and $\langle b_1, b_{11} \rangle$ are both 50,000, the branch probabilities of the two branches are both 0.5. After obtaining the branch probabilities, we can calculate the path probabilities of different basic blocks. For instance, the statistical path probability of b_5 is calculated as

$0.5 \times 0.3 \times 0.3 = 0.045$. Given the high throughput of fuzzing and the large number of random samples generated over time, it is reasonable and accurate to calculate branch and path probabilities based on statistical branch hits.

3.1.2 Calculation of probability-based distance. After obtaining the path probabilities of basic blocks, we combine them with BB distances to calculate the probability-based distances. The design is based on two considerations: (1) the probability-based distance is positively correlated with distance and negatively correlated with path probability, (2) introducing a factor of path probability to establish both an upper bound and a lower bound for the distance. This allows us to control the impact of path probability and amplify the effect of changes in path probability, as the probability-based distance will exponentially change with path probability.

$$d_p(m, T_b) = d_b(m, T_b) \cdot c^{-P(path_m)} \quad (3)$$

Where $d_p(m, T_b)$ denotes the probability-based distance, T_b denotes the target basic block, $d_b(m, T_b)$ denotes the BB distance. $c^{(-P(path_m))}$ denotes the factor of path probability to establish both an upper bound ($d_b(m, T_b)$) and a lower bound ($\frac{c}{d_b(m, T_b)}$) for the distance. $P(path_m)$ denotes the path probability of m , and c is a constant which is greater than 1.

3.1.3 Calculation of seed distance. Up to now, almost all existing DGF techniques have used the arithmetic mean of all or part of the BB distances to calculate the seed distance. However, we have observed that in the seed's path, there are some basic blocks that are very close to or have already reached the target sites. These basic blocks contribute more to reaching and testing the target sites and we name them as **critical basic blocks**. Since the arithmetic mean mainly reflects the general level of the population or the central tendency of the distribution [35], it cannot reflect the existence of critical basic blocks in the path. **Therefore, we use the geometric mean, which is more sensitive to the minimum value, to calculate the seed distance.** For example, in Figure 3, Trace A ($\langle b_1, b_2, b_3, b_5, b_8, b_{10} \rangle$) is covered by Seed A, Trace B ($\langle b_1, b_{11}, b_{13}, b_{15} \rangle$) is covered by Seed B, and b_{10} and b_{14} are the target basic blocks. Based on the arithmetic mean, the seed distance of Seed A ($((0 + 1 + 2 + 3 + 4 + 3)/6 = 2.16)$) is greater than the seed distance of Seed B ($((1 + 2 + 3)/3 = 2)$), resulting in Seed B being preferred. However, since Seed A can reach the target basic block, prioritizing Seed A is more reasonable. Given using the geometric mean, the seed distance of Seed A ($(\sqrt[6]{0 \times 1 \times 2 \times 3 \times 4 \times 3} = 0)$) will be smaller than the seed distance of Seed B ($(\sqrt[3]{1 \times 2 \times 3} = 1.81)$). We can see that, in this example, the geometric mean more accurately reflects the presence of critical basic blocks than the arithmetic mean. For this reason, we use the geometric mean to calculate the seed distance.

$$d_s(s, T_b) = \begin{cases} 0, & \text{if } d_p(m_i, T_b) == 0 \wedge m_i \in \xi_b(s) \\ \frac{1}{|\xi_b(s)|} \sqrt[|\xi_b(s)|]{\prod_{m \in \xi_b(s)} d_p(m, T_b)}, & \text{else} \end{cases} \quad (4)$$

Where s denotes the seed, $\xi_b(s)$ denotes the set of basic blocks in the execution path of the seed, and $|\xi_b(s)|$ denotes the number of basic blocks in $\xi_b(s)$. If there is a basic block m_i whose BB distance is 0, it means that the current seed has hit a target basic block. In this case, we consider its seed distance as 0.

Calculation Simplification. To avoid the high overhead caused by the Product and Sqrt operations, we combine Equation (3) and Equation (4) to simplify the calculation of the geometric mean.

$$d_s = \begin{cases} 0, & \text{if } d_p(m_i, T_b) == 0 \wedge m_i \in \xi_b(s) \\ \exp\left\{ \frac{\sum_{m \in \xi_b(s)} (\log(d_b(m, T_b)) - P(path_m))}{|\xi_b(s)|} \right\}, & \text{else} \end{cases} \quad (5)$$

We mainly simplify the second term in Equation (4) based on Equation (3). First, we take the logarithm of both sides of the equation in Equation (3) to convert the Product and Sqrt operations into Summation operations, which yields $\sum_{m \in \xi_b(s)} \log(d_b(m, T_b) \cdot c^{-P(path_m)})$. Then, to optimize the computation process, we set the constant c in Equation (2) to e , so that we can convert the multiplication operation in $\log(d_b(m, T_b) \cdot c^{-P(path_m)})$ into an addition operation, which yields $\sum_{m \in \xi_b(s)} (\log(d_b(m, T_b)) - P(path_m))$. Finally, we exponentiate the equation variables and obtain the optimized formula shown in Equation (5). Through this simplification method, the forking process only needs to perform addition operations, greatly reducing the computation overhead.

3.2 Power Schedule Optimization

Most of the existing DGF techniques use seed distance as the fitness metric, such as AFLGo and WindRanger, which explicitly divides the fuzzing process into the *exploration* phase and *exploitation* phase. The exploration phase is designed to uncover as many paths as possible (like many coverage-guided fuzzers), and DGF in this phase favors seeds that expose new paths and prioritizes them. Then, based on the known paths, the exploitation phase is invoked to drive the engine toward the target code areas. In this phase, DGF prioritizes seeds that are closer to the targets and assigns more energy to them. However, the constraints on the closer seeds' paths may be difficult for DGF to satisfy, leading to a failure in generating new seeds within the limited time budget. Therefore, it is challenging to assign reasonable energy for both phases. With the probability-based distance, we design a Directed Multi-Armed Bandit (i.e., DMAB) model to optimize the power schedule, which can implicitly coordinate the exploration and exploitation in DGF.

The Multi-Armed Bandit (i.e., MAB) problem results from the slot machine with multiple arms. The player plays one of the arms and obtains a reward. The player's main goal is maximizing the rewards in finite trials. Recent works, such as EcoFuzz [19], have applied the Adversarial MAB model to improve CGF, where the arms represent the seeds, and the reward represents the probability of uncovering new paths by mutating a seed. Based on the Adversarial MAB, EcoFuzz assumes that the probability of uncovering new paths decreases as the coverage of CGF increases. However, different from CGF, HyperGo measures the difficulty of covering new branches based on the branch probability of unexplored branches. Since the branch probabilities are only related to the complexity of condition constraints, which is a fixed value, we model the process of HyperGo covering new branches as a *Stochastic Multi-Armed Bandit* problem.

In the stochastic MAB model, there are N fixed parallel arms, and at each time step t , one arm indexed as i , ($i \in K = 1, 2, \dots, N$) is selected to play. After playing arm i , the player receives a reward, and the rewards of each slot machine may follow a fixed probability distribution. Using the greedy algorithm, we tend to select the arm with the highest reward. However, to obtain the global optimum,

we need to explore different arms to evaluate their reward probability and select the arm with the highest reward expectation. In the DMAB model, we map the elements in DGF to rewards and reward probabilities and combine them into reward expectations. Compared to traditional DGF methods, DMAB eliminates the need to explicitly differentiate exploration and exploitation. The assignment of seed energy is determined based on the difficulty of reaching the target sites for each seed, which implicitly incorporates the exploration and exploitation requirement.

3.2.1 Elements in DMAB model. We map the elements in DGF to the DMAB model as follows.

Reward. We consider mutating seed s as playing the slot machine. After mutating the seed s , a new input is generated and a reward is obtained. The value of the reward depends on whether the new input covers a new branch. There are two possible values for the reward: 0 or a value $r(d_s)$ which is negatively related to the seed distance, represented as d_s . The reward of 0 indicates that the new input cannot cover a new branch while the reward of $r(d_s)$ indicates that the new input covers a new branch. Based on a large number of tests, we find that new seeds generated from mutating the seed with shorter distance are more likely to have shorter distances. Thus, we believe that the reward is negatively correlated with the seed distance of seed s . **To exploit the seeds with shorter distances, we prefer the seeds with higher rewards and assign the seeds more energy.**

Reward probability. To estimate the reward expectation, we need to evaluate the probability distribution of the reward. Whether DGF can cover new branches is related to whether the input can satisfy the constraint conditions of unexplored branches in the path. Therefore, we use the average branch probability of all unexplored branches in the path of seed s to evaluate the probability of the fuzzer covering an unexplored branch through mutating seed s , represented as reward probability. **To explore more paths, we prefer the seeds that have higher probabilities of covering new branches and assign the seeds more energy.**

Reward expectation. We combine the reward and reward probability to evaluate the reward expectation. The design of the reward expectation is:

$$E(r) = \frac{1}{d_s(s, T_b)} \cdot \frac{\sum_{br \in \Theta(s)} P(br)}{|\Theta(s)|} \quad (6)$$

Where $d_s(s, T_b)$ denotes the seed distance of the seed s , $\Theta(s)$ denotes the set of unexplored branches in the path of s , $P(br)$ denotes the branch probability. The first term in Equation 6 represents the reward, which is negatively correlated with $d_s(s, T_b)$. The second term represents the reward probability, which is equal to the average branch probability of all unexplored branches.

Based on Equation (6), the DMAB model can dynamically coordinate the exploitation and exploration. As the fuzzing campaign launches, all seeds have not been sufficiently mutated and they have similar reward probabilities. Therefore, the DMAB model will exploit closer seeds with higher reward expectations. As fuzzing progresses, the closer seeds are sufficiently fuzzed and their reward probabilities will decrease as the number of mutations increases. According to Equation (6), the reward expectation of these closer seeds will gradually become lower than that of the seeds with higher

reward probability. As a result, the DMAB model will assign more energy to the seeds with higher reward probabilities to explore more new paths, implicitly switching to exploration.

3.2.2 Design of power schedule. After obtaining the reward expectations of all seeds, we optimize the power schedule based on the reward expectations to coordinate exploration and exploitation in DGF. We design the power schedule for two objectives. Firstly, the fuzzer should assign more energy to seeds with higher reward expectations, and less energy to seeds with lower reward expectations. Secondly, the energy of seeds can be adaptively adjusted with the progress of fuzzing. Based on these two objectives, we redesign the power schedule in HyperGo.

Firstly, we normalize the reward expectations of all seeds.

$$\tilde{E}(r) = \frac{E(r) - \min E}{\max E - \min E} \quad (7)$$

Where $\min E$ denotes the minimum reward expectation among all seeds, and $\max E$ denotes the maximum reward expectation among all seeds. Then, we integrate the normalized reward expectations with AFL's power schedule to form an optimized power schedule.

$$P(s, T_b) = \begin{cases} P_{afl}(s) \cdot 2^{10 \cdot \tilde{E}(r) - 5}, & \text{if } \Theta(s) \neq \emptyset \\ \frac{P_{afl}(s)}{32}, & \text{if } \Theta(s) = \emptyset \end{cases} \quad (8)$$

Where $P_{afl}(s)$ denotes seed energy assigned by AFL's power schedule, $P(s, T_b)$ denotes the finally assigned seed energy after optimization. AFL's power schedule assigns basic energy to the seed based on the seed's characteristics, such as the seed's execution speed and the size of its bitmap. By taking into account both the seed's characteristics and the reward expectation, we integrate AFL's power schedule and reward expectations to design the optimized power schedule. Moreover, to prevent the overuse of seeds and neglect of seeds that may contribute more to reaching target sites, we design the term $2^{10 \cdot \tilde{E}(r) - 5}$ to control the adjustment of AFL's assigned energy within the range of $[1/32, 32]$.

As fuzzing progresses, the number of unexplored branches and branch probabilities will change. This means that the reward expectations of all seeds will also change constantly. This allows HyperGo to dynamically assign seed energy and balance the trade-off between exploration and exploitation in a more accurate way. In Section 5.4, we demonstrate the effectiveness of the DMAB model in steering DGF to reach the target sites.

3.3 Optimized Symbolic Execution Complementary Scheme

To address the issues of directed hybrid fuzzing mentioned in Section 2.1, we design an Optimized Symbolic Execution Complementary (i.e., OSEC) scheme. In the OSEC scheme, we take three measures: pruning the unreachable branches, pruning the unsolvable branches, and dynamically prioritizing the symbolic execution of seeds. Algorithm 1 represents the workflow of the OSEC scheme.

In Algorithm 1, Ω_s represents the set of all seeds provided by DGF. D represents a dictionary containing (*seed index*, *seed distance*, *average branch probability*) triplets. Based on the seed's index, we can obtain the seed distance and the average branch probability of all unexplored branches in the seed's path (represented as $\tilde{P}(\Theta(s))$). ψ_s represents the set of all new seeds generated by the symbolic

Algorithm 1 The Workflow of OSEC Scheme

```

Input:  $\Omega_s, D$ 
Output:  $\psi_s$ 
1: while  $s \in \Omega_s$  do
2:    $d_s, \bar{P}(\Theta(s)) \leftarrow D(s)$ 
3:    $\text{Score}(s) = \text{Cal\_Sco}(d_s, \bar{P}(\Theta(s)), \bar{S}\bar{A}(\Theta(s)))$ 
4:   Sort( $\Omega_s$ )
5: end while
6: while true do
7:    $s \leftarrow \text{Top\_Rank}(\Omega_s)$ 
8:    $\Theta(s) \leftarrow \text{Sym\_Exe}(s)$ 
9:   while  $br \in \Theta(s)$  do
10:    if  $br$  is unreachable or  $br$  is unsolvable then
11:      delete  $br$  from  $\Theta(s)$ 
12:    else
13:       $\text{new\_seed} \leftarrow \text{Constraint\_Solve}(\tau_{br})$ 
14:       $\psi_s = \psi_s \cup \{\text{new\_seed}\}$ 
15:    end if
16:  end while
17:   $\text{Score}(s) = \text{Cal\_Sco}(d_s, \bar{P}(\Theta(s)), \bar{S}\bar{A}(\Theta(s)))$ 
18:  Sort( $\Omega_s$ )
19: end while

```

executor, $\bar{S}\bar{A}(\Theta(s))$ represents the average number of solving attempts for unexplored branches, and τ_{br} represents the set of the unexplored branch's path constraints. Before the symbolic execution of seeds, the seed's $\bar{P}(\Theta(s))$ is calculated by DGF based on Equation (6) and the $\bar{S}\bar{A}(\Theta(s))$ is initialized to 1.

Firstly, the OSEC calculates the priority scores based on the seed distance, the average branch probability, and the average solving attempts. The priority scores are used to sort the seeds in descending order (Lines 2-5). Then, the OSEC continuously selects the seed with the highest priority score from Ω_s , tracks the execution path of the seed, and identifies all unexplored branches to form the set $\Theta(s)$ (Lines 7-8). Next, the OSEC determines whether the unexplored branches are unsolvable or unreachable. If so, the OSEC prunes these branches. If not, the OSEC invokes the constraint-solver to solve the path constraints of these branches to generate new seeds. The new seeds are added to the set of new seeds ψ_s (Lines 9-16). After the symbolic execution of the seed, the value of d_s , $\bar{P}_{br}(\Theta(s))$, and $\bar{S}\bar{A}(\Theta(s))$ will all change. Therefore, we recalculate the priority score of the seed and re-sort all seeds (Lines 17-18). In the following sections, we will introduce in detail how to prune branches and calculate seed priority scores.

3.3.1 Pruning the unreachable branches. To avoid solving path constraints of the branches that do not contribute to reaching the target sites (i.e., unreachable branches), we need to prune the unreachable branches. We determine whether an unexplored branch is an unreachable branch based on the reachability of its destination basic block. We assume that if the destination basic block of a branch is unreachable, all successor basic blocks of that destination basic block are also unreachable. Thus, we consider this branch as an unreachable branch and give up solving its path constraints.

To determine whether an unexplored branch, represented as $\langle m_s, m_d \rangle$, is unreachable, the OSEC loads the mappings of basic block addresses and BB distances ($\langle BB_add, BB_dis \rangle$) provided by the static analyzer to obtain the BB distances of all basic blocks. Then, the OSEC checks the BB distance of m_d (whether $d_b(m_d, T_b) \geq 0$) to determine the reachability of branch $\langle m_s, m_d \rangle$. If branch

$\langle m_s, m_d \rangle$ is unreachable, the symbolic executor will abandon solving this branch and prune it from the set of unexplored branches.

3.3.2 Pruning the unsolvable branches. To alleviate the issue of solving path constraints for the branches that cannot be solved (i.e., unsolvable branches) within a limited time budget, we need to prune the unsolvable branches. When solving the path constraints of a branch, we make two basic assumptions. (1) The time budget for solving the path constraints of each branch has a lower bound (e.g., 5s) and an upper bound (e.g., 15min). The time budget increases with the number of solving attempts, up to the upper limit. (2) If the symbolic executor fails to solve a branch due to the complexity of the branch's path constraints, all subsequent branches of that unsolvable branch are also unsolvable since they have more path constraints than the unsolvable branch.

Based on these two assumptions, we can prune the unsolvable branches. Firstly, we dynamically adjust the time budget within the ranger of $[lower_bound, upper_bound]$ according to the solving attempts. Based on empirical experience, we increase the time budget by 1 minute after each attempt. If the branch cannot be solved within the upper limit time budget, we consider it as an unsolvable branch and give up solving it. Secondly, during the symbolic execution of a seed, we would record the solving results (e.g., success or failure) of the unexplored branches that have been identified. Then, before solving each branch, we check whether its predecessor branch is unsolvable. If unsolvable, based on the second assumption, the path constraints of this branch are too complicated for the symbolic executor to solve within the limited time budget, and thus the branch is regarded as an unsolvable branch. Through these two steps, we prune the unsolvable branches to alleviate the pressure of constraint solving.

3.3.3 Prioritizing the symbolic execution of seeds. To achieve a complementary integration of DGF and SE, we need to dynamically adjust the order of seeds for symbolic execution. Due to its high fuzzing throughput, DGF can quickly cover paths with easy-to-satisfy path constraints. In contrast, SE has the excellent constraint-solving ability to generate inputs that satisfy complex path constraints. To fully leverage the respective strengths of DGF and SE, we want (1) both SE and DGF to prioritize seeds with shorter seed distances, (2) SE to prioritize solving unexplored branches that are difficult for DGF to cover, and (3) SE to prioritize seeds with fewer solving attempts and lower time budgets. We calculate the priority scores of different seeds based on these three considerations and adjust the order of seeds for symbolic execution accordingly.

Firstly, similar to the method of evaluating reward probability in Section 3.2, we use the branch probability of unexplored branches to evaluate the difficulty of the fuzzer covering the unexplored branches through mutating seed s .

$$EDF(s) = \frac{\sum_{br \in \Theta(s)} P(br)}{|\Theta(s)|} \quad (9)$$

Where $EDF(s)$ denotes the estimated difficulty. Similarly, we use the average branch probability of all unexplored branches in the path of seed s as the estimated difficulty. Moreover, based on the branch probability calculation method in Section 3.1, the branch probabilities of unexplored branches are all greater than 0.

Then, we evaluate the solving difficulty of branches based on the number of solving attempts. That is, more solving attempts indicate that the symbolic executor has more difficulty in solving the path constraints of the branch. We use the average solving attempts of all unexplored branches in the path of seed s to evaluate the solving difficulty of the seed's branches.

$$EDS(s) = \frac{\sum_{br \in \Theta(s)} SA(br)}{|\Theta(s)|} \quad (10)$$

Where $EDS(s)$ denotes the estimated difficulty, $SA(br)$ denotes the number of solving attempts of the unexplored branch.

Based on $EDF(s)$, $EDS(s)$, and $d_s(s, T_b)$, we score the seeds to determine their order for symbolic execution. To ensure that the three indicators have the same weight in affecting the priority score of seeds, we use a normalization method as shown in Equation (7) to calculate their normalized value. Then, we can calculate the priority score of different seeds.

$$Score(s) = \frac{\widetilde{EDF}(s)}{\widetilde{EDS}(s) \cdot \widetilde{d}_s(s, T_b)} \quad (11)$$

Where $\widetilde{EDF}(s)$, $\widetilde{EDS}(s)$ and $\widetilde{d}_s(s, T_b)$ are the normalized value. After obtaining the priority scores of all seeds, the OSEC scheme will prioritize the seeds with higher scores for symbolic execution. Moreover, since the three factors used to calculate the priority scores, $EDF(s)$, $EDS(s)$, and $d(s, T_b)$, are changing dynamically, the OSEC scheme will adaptively adjust the order of symbolic execution of the seeds. By this method, the OSEC scheme dynamically prioritizes the optimal seeds whose unexplored branches are hard for the fuzzer to penetrate through, are more likely to be solved by the symbolic executor, and are closer to targets.

During the symbolic execution, the symbolic executor will constantly attempt to solve the unexplored branches in the seeds' paths and generate new interesting seeds for DGF.

4 IMPLEMENTATION

The implementation of HyperGo mainly consists of three components: a static analyzer, a fuzzer, and a symbolic executor. For the static analyzer, we leverage the static analysis framework LLVM 11.0 and Clang 11.0 and use the LLVM IR to instrument the program. The fuzzer is built on AFL 2.52b, and the symbolic executor is built on Symcc. The implementation part of HyperGo is implemented with about 2000 lines of C/C++ and RUST code. HyperGo is publicly available on our website (<https://gitee.com/paynelin/hypergo>).

5 EVALUATION

To evaluate the effectiveness of HyperGo, we conducted experiments aiming to answer four research questions:

RQ1: What about the performance of HyperGo in terms of reaching the target sites?

RQ2: What about the performance of HyperGo in terms of exposing the vulnerabilities in the target sites?

RQ3: How probability-based distance, the DMAB model, and the OSEC scheme take effect in the overall performance of HyperGo?

RQ4: Is the probability-based fitness metric effective in finding better seeds for directed fuzzing?

RQ5: What about the performance of HyperGo in terms of discovering new vulnerabilities?

5.1 Evaluation Setup

Evaluation Criteria. We mainly use two types of criteria to evaluate the performance of different fuzzing techniques.

(1)Time-to-Reach (TTR) is used to evaluate the time spent on generating the first input which can reach the specific target site.

(2)Time-to-Expose (TTE) is used to evaluate the time spent on exposing the (known or undisclosed) vulnerabilities in the target sites. When a crash is observed at the target site, it indicates that the fuzzer has successfully exposed the vulnerability.

Evaluation Benchmarks. We selected two datasets and 7 real-world programs with potential vulnerabilities.

(1) UniBench [23] provides real-world programs of different types for testing, which is widely used by state-of-the-art fuzzers, such as WindRanger. To answer RQ1, RQ2, and RQ3, we tested 16 programs from UniBench and set 5 target sites for each program. Notably, we preferred the code locations that are difficult for CGF to reach (i.e., require CGF more than 1 hour to reach) as target sites to better distinguish the performance of different fuzzers.

(2) AFLGo test suite [4] was proposed in AFLGo's paper and website to evaluate the directness of DGF, and it had been used as a benchmark by many state-of-the-art directed fuzzers (e.g., Hawkeye and WindRanger). To answer RQ2, we selected it as the benchmark.

(3) Additional real-world programs. In addition to UniBench, we add another 9 real-world programs to construct a new testbench (all the programs are listed in Table 4 in the Appendix). To answer RQ4, we used sanitizers (e.g., UBSAN [2], ASAN[37]) to label the target sites for the testbench and tested them with HyperGo.

Baselines. In our evaluation, we compared HyperGo with the state-of-the-art directed greybox fuzzers that are publicly available by the time of writing this paper, including WindRanger, BEACON, ParmeSan, and AFLGo. To conduct the incremental experiments, we combined AFLGo with SymCC to form a new directed hybrid fuzzer, which is called AFLGoSy, as the baseline.

Experiment Settings. We conducted the experiments on the machine equipped with Intel(R) Xeon(R) Gold 6133 CPU @ 2.50GHz with 80 cores and used Ubuntu 20.04 LTS as the operating system. All the experiments were repeated 5 times within a time budget of 24 hours. When testing the programs from UniBench and AFLGo test suite, we used the seeds in the BenchMarks' recommended seed corpus as initial seeds. For experimental results analysis, we utilize the Mann-Whitney U test (p-value) to measure the statistical significance and the Vargha-Delaney statistic (\hat{A}_{12}) [3] to measure the probability of one technique performing better than another.

5.2 Reaching Target Sites

To answer RQ1, we tested 16 programs from UniBench, with a total of 80 target sites, and evaluated the TTR of different fuzzers. We set the timeout threshold as 24 hours. Owing to the page limit, detailed results were listed in Table 5 in the Appendix. According to the results of TTR, HyperGo can reach the most (80/80) target sites compared to AFLGo (25/80), AFLGoSy (33/80), BEACON (11/80), WindRanger (20/80), and ParmeSan (12/80) within the time budget. Moreover, on most of the target sites (74/80), HyperGo outperforms

all other fuzzers and achieves the shortest TTR. In terms of mean TTR of reaching the target sites, HyperGo demonstrates 38.47 \times , 30.89 \times , 28.52 \times , 106.09 \times and 143.22 \times speedup compared to AFLGo, AFLGoSy, BEACON, WindRanger, and ParmeSan, respectively. We conducted both the Mann-Whitney U test (p-value) and the Vargha-Delaney test (\hat{A}_{12}), all the p-values are less than 0.01, and the mean \hat{A}_{12} against AFLGo, AFLGoSy, BEACON, WindRanger, and ParmeSan are 0.88, 0.85, 0.92, 0.86, and 0.91, respectively. Based on the above analysis, we can conclude that **HyperGo can reach the target sites faster than baseline fuzzers.**

To reflect the results in a straight way, we use bar charts to visualize the results. In Figure 4, the x-axis represents the target site ID (1-80), the y-axis represents the total TTR of all fuzzers in minutes, and a shorter bar indicates a shorter TTR. Since some fuzzers cannot compile some programs or reach the target sites within the 24-hour time budget, resulting no TTR. To distinguish these cases, the TTR of such a case is represented as 1500 min in Figure 4. From the figure, we can clearly see that the blue bars are much shorter than the other bars, which means that HyperGo can reach most of the target sites faster than the baseline fuzzers.

5.3 Exposing vulnerabilities

To answer RQ2, following BEACON and WindRanger, we used the AFLGo testsuite and set the known vulnerabilities with CVE IDs in the programs as the target sites. The information on target sites and the TTE results are presented in Table 1. As Table 1 shows, among the 20 vulnerabilities, HyperGo exposed the most (18) compared to AFLGo (14), AFLGoSy (15), BEACON (13), WindRanger (16), and ParmeSan (14). Besides, on most of the target sites (15/20), HyperGo outperformed all the baseline fuzzers and achieved the shortest TTE. With respect to the mean TTE of exposing vulnerabilities, HyperGo demonstrated 3.44 \times , 3.63 \times , 4.10 \times , 3.26 \times and 3.00 \times speedup compared to AFLGo, AFLGoSy, BEACON, WindRanger, and ParmeSan, respectively. All p-values were less than 0.05, and the mean \hat{A}_{12} against AFLGo, AFLGoSy, BEACON, WindRanger, and ParmeSan were 0.84, 0.82, 0.79, 0.76, and 0.80, respectively. Based on the above analysis, we can conclude that **HyperGo can expose known vulnerabilities faster than the baseline fuzzers.**

To show why HyperGo can expose the vulnerabilities faster, we used CVE-2017-9047 to conduct a case study. As Listing 1 shows,

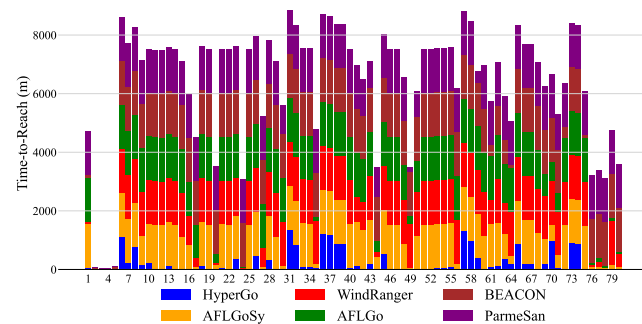


Figure 4: TTR of AFLGo, AFLGoSy, BEACON, WindRanger, ParmeSan, and HyperGo on the UniBench.

the function `xmlSprintfElementContent()` is supposed to recursively dump the element content definition into a char buffer `buf` of size `size`. If `content->type` is `XML_ELEMENT_CONTENT_ELEMENT`

```

1 int xmlValidateOneElement(){
2   if (elemDecl->contModel == NULL)
3     ret = xmlValidBuildContentModel(ctxt,elemDecl);
4 }
5 int xmlValidBuildContentModel(){
6   ...
7   xmlSprintfElementContent();
8 }
9 void xmlSprintfElementContent(){
10  int len = strlen(buf);
11  switch (content->type) {
12    ...
13    case XML_ELEMENT_CONTENT_ELEMENT:
14      strcat(buf, (char *) content->prefix);
15      if(size-len<xmlStrlen(content->name)+10)
16        ...
17    }
18  }

```

Listing 1: The example of CVE-2017-9047.

(Line 13), `content->prefix` is appended to `buf` (Line 14) and then `content->name` is written to the buffer, causing the length of `buf` changed. However, in Line 15, the check for whether `content->name` actually fits also uses `len` rather than the updated buffer length `strlen(buf)`. This allows the attacker to tamper size to a large number that is beyond the allocated memory size and overflow the buffer.

To expose this vulnerability, a fuzzer has to satisfy the condition at Line 2 to reach the callsite and the root cause of this vulnerability (marked as red). Due to the randomness of mutation strategies in fuzzing, it is challenging to generate inputs that satisfy these complex constraints within a limited time budget. As a result, AFLGo, WindRanger, BEACON, and ParmeSan failed to expose the vulnerability within 24 hours. Since AFLGoSy did not prioritize solving

Table 1: The results of TTE on AFLGo testsuite

Prog.	CVE-ID	AFLG	AFLS	BEAC	Wind	Parm	HyGo
binutils _{2.26}	2016-4487	2.33m	2.42m	0.63m	1.21m	0.95m	1.42m
	2016-4488	4.23m	3.60m	32.1m	3.32m	2.62m	2.12m
	2016-4489	3.36m	4.11m	2.98m	5.88m	2.31m	1.89m
	2016-4490	1.15m	1.81m	2.35m	2.63m	0.82m	1.68m
	2016-4491	448m	389m	258m	298m	212m	69.3m
	2016-4492	10.8m	13.2m	43.6m	7.47m	4.33m	3.94m
libmng _{4.48}	2016-6131	348m	236m	292m	318m	244m	101m
	2018-8807	331m	218m	267m	171m	301m	68.3m
	2018-8962	234m	271m	163m	121m	198m	43.7m
	2018-11095	T.O.	914m	252m	1311m	T.O.	118m
LibPNG _{1.5.1}	2018-11225	T.O.	T.O.	438m	996m	T.O.	202m
	2011-2501	10.2m	12.3m	N/A	7.81m	4.53m	2.16m
	2011-3328	69.1m	54.3m	N/A	49.3m	193m	21.1m
xmlint _{2.9.4}	2015-8540	0.88m	1.19m	N/A	0.96m	3.41m	2.65m
	2017-9047	T.O.	T.O.	T.O.	T.O.	T.O.	983m
	2017-9048	T.O.	T.O.	T.O.	T.O.	T.O.	T.O.
Lrzip _{0.631}	2017-9049	T.O.	T.O.	T.O.	T.O.	T.O.	635m
	2017-9050	T.O.	T.O.	T.O.	T.O.	T.O.	T.O.
	2017-8846	348m	284m	156m	223m	466m	69.4m
speedup	2018-11496	201m	226m	98.1m	169m	126m	33.9m
		3.44 \times	3.63 \times	4.10 \times	3.26 \times	3.00 \times	-
mean \hat{A}_{12}		0.84	0.82	0.79	0.76	0.80	-
mean p-values		0.009	0.013	0.006	0.026	0.008	-

the path constraint involving Line 2 nor dynamically adjust the time budget of constraint-solving, its symbolic executor could not generate test cases to execute `xmlSprintfElementContent()`, either. As a result, it also failed to expose the vulnerability. In contrast, HyperGo’s OSEC scheme prioritizes solving the path constraint involving Line 2 based on distance and solving difficulty, it dynamically adjusts the time budget for constraints solving during multiple attempts. Thus, HyperGo was able to execute `xmlSprintfElementContent()` within 769 minutes and generate a test case that satisfies the root cause in 983 minutes, in which `content->type` equals `XML_ELEMENT_CONTENT_ELEMENT`.

5.4 The Impact of the Optimizations on the Overall Performance

To answer RQ3, we employed two methods to evaluate the impact of the optimizations. Firstly, we conducted incremental experiments to evaluate the effects of the three optimizations on HyperGo’s overall performance. Secondly, we used some intermediate experimental data to reflect the effects of different optimizations.

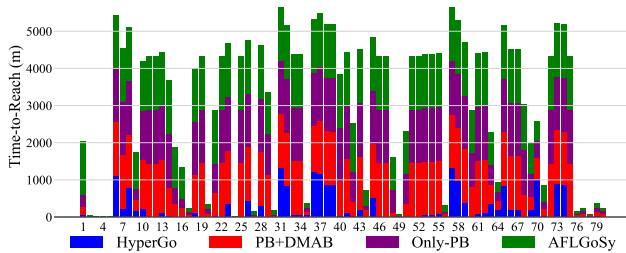


Figure 5: Incremental experiment results of AFLGoSy, Only-PB, PB+DMAB, and HyperGo using TTR.

5.4.1 Incremental experiments. We use AFLGoSy as the base tool. Since the DMAB model and OSEC scheme are based on the probability-based distance, disabling the probability-based distance calculation module will disable the other modules. Thus, we first add the probability-based distance module to AFLGoSy to implement a new tool (i.e., Only-PB). Then, we add the DMAB model to Only-PB, forming a new tool (i.e., PB+DMAB). Finally, we add the OSEC scheme to PB+DMAB to form HyperGo. In the incremental experiment, the configurations and the target sites remain unchanged as Section 5.2. According to the TTR results, Only-PB (35), PB+DMAB (40), and HyperGo (80) can all reach more target sites than AFLGoSy (33). Moreover, Only-PB, PB+DMAB, and HyperGo outperform AFLGoSy by 1.33×, 1.84×, and 30.89× respectively in the average TTR of reaching the target sites. Detailed results are listed in Table 6 in the Appendix. These results demonstrate that **each optimization has a significant impact on reducing TTR, and using one or two optimization strategies (Only-PB and PB+DMAB) are far less effective than using all three optimization strategies simultaneously (HyperGo)**. To visualize the experimental results, the results of TTR are shown in Figure 5, in which the x-axis represents the target site ID (1-80), and the y-axis represents the total TTR of all fuzzers in minutes.

5.4.2 Intermediate data analysis. In addition to the incremental experiments, we analyzed the intermediate experimental data to

more intuitively illustrate the effects of different optimizations. We used three metrics for analysis: (1) The number of reachable seeds generated by fuzzers, i.e., *FRseeds*. If the fuzzer can generate more reachable seeds, it indicates that the fuzzer can explore more paths and find an optimal path to reach the target sites. (2) The number of reachable seeds generated by the symbolic executor, i.e., *SRseeds*. The more SRseeds indicate that the symbolic executor can provide more assistance to the fuzzer to cover new paths. (3) The number of new seeds generated by mutating the SRseeds, i.e., *FSRseeds*. After receiving the reachable seeds provided by the symbolic executor (i.e., SRseeds), the fuzzer will mutate them to explore new code areas and generate new seeds. The larger number of FSRseeds indicates that the symbolic executor can help the fuzzer break through complex constraints and explore code areas that are hard for the fuzzer to reach. We evaluated AFLGoSy, Only-PB, PB+DMAB, and HyperGo on the 16 programs from UniBench and counted the number of these three seed types, which are presented in Table 2.

From Table 2, we can observe that for the average number of FRSeeds, both Only-PB (5112) and PB+DMAB (7313) are much greater than that of AFLGoSy (2479). This indicates that the probability-based distance and DMAB model can effectively explore more paths to reach the target sites. As for the SRseeds and FSRseeds, those of HyperGo are much greater than those of other fuzzers. This indicates that the OSEC scheme significantly improved the efficiency of symbolic execution, which helped and tested code areas that are difficult for the fuzzer to reach. Furthermore, according to the number of all three seed types, we can see that the performance of HyperGo, which uses all three optimizations, is significantly better than that of the fuzzers using only one or two strategies. This implies that the overall design of HyperGo, including the new fitness metric, optimized power schedule, and OSEC scheme, works in a complementary way and achieves significant improvement.

5.5 Branch probability distribution analysis of the unexplored branches

In the incremental experiments and intermediate data analysis, we observe that HyperGo can reach target sites faster than AFLGoSy and explore more paths leading to target sites. To verify whether the seeds preferentially selected by HyperGo using probability-based optimizations are better than those non-probability tools (RQ4), we analyze the high-priority seeds generated by HyperGo and AFLGoSy when testing UniBench. First, we divide the fuzzing process into 24 intervals, and each lasts for one hour. At each time point, such as 1-hour, we collect the top 100 seeds with the highest priority from the programs under test. Hence, at each time point, we collect 1600 seeds with the highest priority from the 16 programs of UniBench. Then, we analyze the probability distribution of the seeds’ unexplored branches.

Table 2: Intermediate data analysis using different seeds

Fuzzers	FRSeeds	SRseeds	FSRseeds
AFLGoSy	2479	18	98
Only-PB	5112	22	86
PB+DMAB	7313	29	103
HyperGo	12432	267	843

The results are shown in Figure 6, which includes two subfigures, depicting the unexplored branch probability distribution for HyperGo and AFLGoSy, respectively. For each subfigure, the x-axis represents the index of unexplored branches, the y-axis represents different time points, and the z-axis represents the branch probability. Each point (x, y, z) on the coordinate axis represents the branch probability of the x^{th} unexplored branch at y^{th} time point. Both Figure 6(a) and Figure 6(b) contain 24 branch probability distribution curves, corresponding to the 24 time points. To better illustrate the results, we sorted all branch probabilities and placed unexplored branches with higher probabilities closer to the middle. Then, to better visualize the overall branch probability, we performed curve fitting on all branch probabilities, resulting in a curve resembling a Gaussian distribution. We can obtain the maximum branch probability of different time points by identifying the highest point in the middle of the curve, and we can evaluate the overall branches' probabilities according to the overall height of the curve.

From Figure 6, we can observe that the height of the AFLGoSy and HyperGo curves decreases gradually with the increasing of time, indicating the branch probability of all unexplored branches decreases during the fuzzing process. This is because the fuzzer is getting difficult to satisfy the branch conditions of unexplored branches as the fuzzing iterations increase. Furthermore, it is noteworthy that HyperGo's unexplored branches generally exhibit higher branch probabilities than AFLGoSy's. This indicates that the overall seed quality of HyperGo is better than that of AFLGoSy, making HyperGo can explore more paths toward target sites. This can be attributed to HyperGo's probability-based optimizations, which prioritize seeds that are more likely to cover unexplored branches as compared to AFLGoSy. Hence, we can conclude that **the probability-based fitness metric employed by HyperGo plays a crucial role in discovering better seeds, which are more likely to cover unexplored branches so as to explore more paths toward target sites.** This is essential for achieving faster attainment of the target sites in directed fuzzing.

5.6 Discovering new vulnerabilities

To answer RQ4, we used HyperGo to test real-world programs. We first used sanitizers (i.e., UBSAN [2] and ASAN[37]) to locate and label potential vulnerabilities as the target sites. Then, we run HyperGo for 24 hours to detect new vulnerabilities. Finally, HyperGo discovered 37 undisclosed vulnerabilities from 7 real-world programs. The information about these vulnerabilities is presented

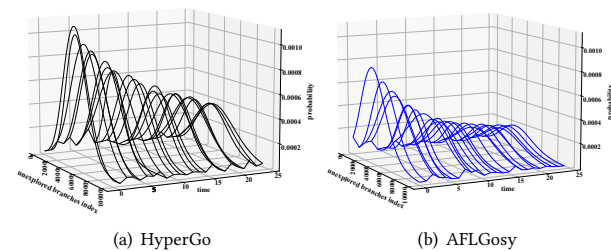


Figure 6: Branch probability distribution of HyperGo and AFLGoSy.

in Table 3. From the table, we can see that the new vulnerabilities involve heap-buffer-overflow, out-of-bounds read/write, stack-overflow, Null pointer dereference, and memcpy-param-overlap.

We also used the baseline fuzzers to detect them. As a result, among the 37 discovered vulnerabilities, 17 could also be detected by AFLGo, 20 by AFLGoSy, 10 by BEACON, 17 by WindRanger, and 8 by ParmeSan. As for the reason that the vulnerabilities could not be detected, one is that the fuzzer could not run the program or obtain the distance information for analysis, while the other reason is the vulnerability could not be triggered within the time budget. From the above result, we can conclude that **HyperGo can detect new vulnerabilities from real-world programs, and it outperforms the baseline fuzzers.**

```

1  static gboolean gdk_pixbuf_pcx_load_increment{
2  if(context->current_task==PCX_TASK_LOAD_DATA) {
3  switch(context->bpp) {
4  ...
5  case 4:
6  retval=pcx_increment_load_data_4(context);
7  static gboolean pcx_increment_load_data_4(){
8  ...
9  p=read_pixel_4(planes[0], i)&&0xf;
10 }
11 }
12 }
13 }
14 static gchar read_pixel_4(){
15 if(!(offset % 2))
16 etval = data[offset] >> 4;
17 }

```

Listing 2: Example of a heap-overflow in gdk-pixbuf 2.31.1.

We use the example in Listing 2 as a case study to explain why HyperGo could discover more vulnerabilities than the baseline fuzzers. Listing 2 shows a heap-overflow vulnerability in function `read_pixel_4()` of `gdk-pixbuf 2.31.1`. At Line 10, due to the lack of range restriction on variable `offset`, if the value of `offset` exceeds the memory allocated for the array `data`, a heap overflow would occur. To trigger this vulnerability, the fuzzer needs to generate inputs that satisfy both the path constraints at Line 1 and Line 3 and satisfy the root cause of the vulnerability. Within the time budget of 24 hours, AFLGo, AFLGoSy, WindRanger, and BEACON failed to generate specific inputs that satisfy all three conditions simultaneously to trigger this vulnerability. Based on three optimization strategies, HyperGo was able to reach Line 10 more efficiently and generated an input that triggers the vulnerability within 160 minutes.

6 DISCUSSION

HyperGo adopts three optimizations to enhance the directedness, including the probability-based distance, the DMAB model, and the OSEC scheme. Specifically, the probability-based distance prioritizes the optimal seeds which have shorter seed distances and higher path probabilities. The DMAB model optimizes the power schedule, which implicitly balances the exploitation of seeds with short distances and the exploration of more reachable seeds. The OSEC scheme combines DGF and SE in a complementary manner. After pruning the unreachable and unsolvable branches, HyperGo prioritizes the symbolic execution of the seeds with higher scores to accelerate the speed of reaching targets. Experiments have proved the effectiveness of HyperGo in reaching the target sites (Section

Table 3: New vulnerabilities detected by HyperGo

No	Prog	Bug function	Bug Type	GSBWPB
1	cflow1.6	symbol.c:302	heap-buffer-overflow	××✓✓×✓
2	gdk-pixbuf-2.31	gdk-pixdata.c:439	heap-buffer-overflow	✓✓✓✓✓✓
3	gdk-pixbuf-2.31	io-qtif.c:437	out-of-bounds read	✓✓✓✓×✓
4	gdk-pixbuf-2.31	io-pcx.c:450	heap-buffer-overflow	×××××✓
5	gdk-pixbuf-2.31	io-pcx.c:528	heap-buffer-overflow	✓✓✓✓×✓
6	gdk-pixbuf-2.31	gdk-pixdata.c:142	heap-buffer-overflow	××✓××✓
7	gdk-pixbuf-2.31	io-ico.c:710	heap-buffer-overflow	✓✓✓✓×✓
8	gdk-pixbuf-2.31	io-ico.c:681	heap-buffer-overflow	✓✓✓✓×✓
9	gdk-pixbuf-2.31	io-ico.c:657	heap-buffer-overflow	×××××✓
10	gdk-pixbuf-2.31	io-ico.c:751	heap-buffer-overflow	✓✓✓✓×✓
11	gdk-pixbuf-2.31	io-pcx.c:253	heap-buffer-overflow	✓✓✓✓×✓
12	gdk-pixbuf-2.31	io-pcx.c:375	heap-buffer-overflow	×✓✓✓×✓
13	gdk-pixbuf-2.31	io-tga.c:441	heap-buffer-overflow	×××✓×✓
14	gdk-pixbuf-2.31	io-tga.c:480	heap-buffer-overflow	×××××✓
15	gdk-pixbuf-2.31	io-ico.c:619	heap-buffer-overflow	×××××✓
16	gdk-pixbuf-2.31	io-tga.c:401	out-of-bounds write	×××××✓
17	gdk-pixbuf-2.31	io-pcx.c:271	heap-buffer-overflow	×××××✓
18	jhead-3.00	jpgguess.c:195	heap-buffer-overflow	××××✓✓
19	jhead-3.00	exif.c:669	out-of-bounds read	×✓×××✓
20	mp3gain-1.5.2	common.c:328	memcpy-param-overflow	✓✓×××✓
21	xpdf-4.00	Stream.c:2919	heap-buffer-overflow	×××××✓
22	xpdf-4.00	gmem.c:140	stack-overflow	×××××✓
23	xpdf-4.00	Stream.c:2760	heap-buffer-overflow	×××××✓
24	xpdf-4.00	gmem.c:311	stack-overflow	×××××✓
25	xpdf-4.00	Lexer.c:489	global-buffer-overflow	✓✓×✓×✓
26	xpdf-4.00	TextOutputDev.c:3065	stack-overflow	✓✓×✓×✓
27	xpdf-4.00	Stream.c:786:	stack-overflow	×××××✓
28	xpdf-4.00	Stream.c:3480	heap-buffer-overflow	✓✓×××✓
29	xpdf-4.00	Dict.c:98	heap-buffer-overflow	×××××✓
30	flvmeta-1.2.1	dump_xml.c:271	out-of-bound read	×××××✓
31	flvmeta-1.2.1	dump_xml.c:151	out-of-bound read	✓✓×✓×✓
32	fig2dev	free.c:152	out-of-bound read	✓✓×✓✓✓
33	fig2dev	free.c:173	out-of-bound read	✓✓×✓✓✓
34	fig2dev	bound.c:525	Null pointer dereference	✓✓×××✓
35	fig2dev	arrow.c:89	Null pointer dereference	✓✓×××✓
36	fig2dev	read.c:1279	out-of-bound read	×✓×✓✓✓
37	fig2dev	read.c:1497	out-of-bound read	✓✓×✓✓✓

1* In the last column, letters G,S,B,W,P, and H represent AFLGo, AFLGoSy, BEACON, WindRanger, ParmeSan, and HyperGo, respectively.

2* '×' denotes that the fuzzer was unable to discover the vulnerability, while '✓' signifies that the fuzzer was able to discover the vulnerability.

5.2), exposing the known vulnerabilities (Section 5.3), and discovering new vulnerabilities (Section 5.6). Moreover, we also proved the effectiveness of the three optimizations (Section 5.4), and we can visually see their effectiveness via branch probability distribution of unexplored branches (Section 5.5).

Different from the SOTA experience-based and intuition-based DGF techniques, HyperGo adopts the probability-based fitness metrics and improvement methods that allowed it to maintain high accuracy across testing different programs in different fuzzing phases. The probability is calculated according to the simple branch hits rather than relying on program analysis or expert knowledge. Therefore, the probability-based fitness metric, the OSEC scheme, and the DMAB model can adaptively select the optimal seeds or optimal paths in current fuzzing phases according to the testing information. Compared to other DGF techniques, HyperGo's adaptability allows it to have higher accuracy when testing most programs.

Threat to validation. Aiming to design an adaptive approach, we adopt several heuristic parameters in HyperGo, which are set empirically (e.g., the setting of the adjustment factor). The values of these parameters might to some extent affect the performance of HyperGo. However, after extensive experiments, we believe the setting of these parameters is stable and suitable for most of the testing scenarios.

7 RELATED WORK

In this section, we focus on discussing the most related works: directed greybox fuzzing and directed hybrid fuzzing.

Directed Grey-box Fuzzing. AFLGo is the first directed greybox fuzzer. It calculates the distances between the seeds and pre-defined targets to prioritize the seeds closer to the targets, which casts reachability as an optimization problem to minimize the distance between the seeds and their targets. Based on AFLGo's idea, Hawkeye [9] proposes the concept of trace similarity and adjusts its seed prioritization, power scheduling, and mutation strategies to enhance directedness. However, Hawkeye suffers the same issues as those of AFLGo when encountering complex path constraints. Even if they assign more energy to the closer seeds, it is difficult for them to satisfy the complex path constraints to cover the path toward target sites. Some directed greybox fuzzers, such as LOLLY [27], Berry [24], UAFL [41], and CAFL [21], propose new fitness metrics, such as sequence similarity, to enhance directedness and detect hard to manifest vulnerabilities. These methods are derived from the analysis of program characteristics or the root causes of different vulnerabilities. Thus, for some specific programs or fuzzing processes, these new fitness metrics may be inaccurate and take a negative effect, which has been discussed in Section 2.2. Other directed greybox fuzzers use data flow information and data conditions information to enhance directedness. WindRanger [13] uses the deviation basic blocks (DBBs) and the data flow information for seed distance calculation, seed mutation, seed prioritization, and power schedule. BEACON [16] leverages a provable path-pruning method to reduce the exploration of infeasible paths. However, due to the limitations of static analysis, BEACON's analysis of infeasible paths (e.g., BEACON cannot recognize indirect calls) may be inaccurate. This can result in the incorrect pruning of some feasible paths, and consequently slowing down the process of reaching target sites. Besides, FuzzGuard [48] uses the deep neural network to extract the features of reachable seeds and filter out the unreachable seeds to improve efficiency. To search the inputs that can reach the target sites, MC^2 designs an asymptotically optimal randomized directed greybox fuzzer that has logarithmic expected execution complexity in the number of possible inputs. However, DGF still suffers from being difficult to penetrate through the hard-to-satisfy path constraints. HyperGo selects the better paths that have fewer hard-to-satisfy path constraints and utilizes symbolic execution to assist DGF to pass through such path constraints.

Directed Hybrid Fuzzing. Directed Hybrid Fuzzing uses the heuristic strategies in hybrid fuzzing to gain directedness. Directed hybrid fuzzers achieve directedness by prioritizing the symbolic execution of reachable seeds or closer seeds. Hydiff [19], SAVIOR [12] and Badger[31] prioritize the seeds that may cause the specific program bug locations as the target sites, and then prioritizes symbolic execution of the seeds which are reachable from more target sites. DrillerGO [18], 1dvul[34], and Berry [25] combine the precision of DSE and the scalability of DGF to mitigate their individual weaknesses. However, modern directed hybrid fuzzers suffer from the limitation of symbolic execution. Since the symbolic executor may fail to solve many unexplored branches or succeed in solving the unreachable branches, such useless constraint solving will have a negative impact on the directedness of directed hybrid fuzzing.

Thus, HyperGo uses the OSEC scheme to prune the unreachable and unsolvable branches and prioritize the symbolic execution of the optimal seeds to better combine DGF and SE.

8 CONCLUSION

In this paper, we propose HyperGo, a probability-based directed hybrid fuzzer. HyperGo adopts the probability-based distance as the fitness metric and an optimized power schedule (namely DMAB model), which can steer DGF to faster reach the target sites through the paths that are easier to re-exercise and closer to the target sites. Using the OSEC scheme, HyperGo combines DGF and SE in a complementary manner to focus on solving constraints toward reachable targets. HyperGo is evaluated on 100 target vulnerabilities of 21 real-world programs from 2 datasets, the experiment results show that HyperGo outperforms the state-of-the-art directed fuzzers (AFLGo, BEACON, WindRanger, and ParmeSan) in reaching target sites and exposing known vulnerabilities. Moreover, HyperGo also discovered 37 undisclosed vulnerabilities and demonstrated its effectiveness in vulnerability discovery.

ACKNOWLEDGMENTS

The authors would like to sincerely thank all the reviewers for your time and expertise on this paper.

REFERENCES

- [1] 2023. *GNU Binutils*. <https://www.gnu.org/software/binutils/>.
- [2] 2023. *Undefined behavior sanitizer - clang 9 documentation*.
- [3] P. Auer, N. Cesa-Bianchi, Y. Freund, and R. E. Schapire. 2002. The nonstochastic multiarmed bandit problem. *SIAM J. Comput.* 32, 1 (2002), 48–77.
- [4] Marcel Böhme. 2023. *Directed Greybox Fuzzing with AFL*.
- [5] A. Arshad S. Weissbacher Blair, W. Mambretti and M. Egele. 2020. HotFuzz: Discovering Algorithmic Denial-of-Service Vulnerabilities Through Guided Micro-Fuzzing. *Network and Distributed System Security Symposium* (2020).
- [6] Marcel Böhme, Van-Thuan Pham, and Abhik Roychoudhury. 2016. Coverage-based Greybox Fuzzing as Markov Chain. In *Proceedings of the 2016 ACM SIGSAC Conference on Computer and Communications Security, Vienna, Austria, October 24-28, 2016*. ACM, 1032–1043.
- [7] Marcel Böhme, Van Thuan Pham, Manh Dung Nguyen, and Abhik Roychoudhury. 2017. Directed Greybox Fuzzing. In *Acm Sigsac Conference on Computer & Communications Security*, 2329–2344.
- [8] Hongxu Chen, Shengjian Guo, Yinxing Xue, Yulei Sui, Cen Zhang, Yuekang Li, Haijun Wang, and Yang Liu. 2020. MUZZ: Thread-aware Grey-box Fuzzing for Effective Bug Hunting in Multithreaded Programs. In *29th USENIX Security Symposium (USENIX Security 20)*. USENIX Association, 2325–2342.
- [9] Hongxu Chen, Yinxing Xue, Yuekang Li, Bihuan Chen, Xiaofei Xie, Xiuheng Wu, and Yang Liu. 2018. Hawkeye: Towards a Desired Directed Grey-box Fuzzer. In *Proceedings of the 2018 ACM SIGSAC Conference on Computer and Communications Security, CCS 2018, Toronto, ON, Canada, October 15-19, 2018*. ACM, 2095–2108. <https://doi.org/10.1145/3243734.3243849>
- [10] Peng Chen and Hao Chen. 2018. Angora: Efficient Fuzzing by Principled Search. In *2018 IEEE Symposium on Security and Privacy, SP 2018, Proceedings, 21-23 May 2018, San Francisco, California, USA*. IEEE Computer Society, 711–725. <https://doi.org/10.1109/SP.2018.00046>
- [11] Peng Chen, Jianzhong Liu, and Hao Chen. 2019. Matryoshka: Fuzzing Deeply Nested Branches. In *Proceedings of the 2019 ACM SIGSAC Conference on Computer and Communications Security, CCS 2019, London, UK, November 11-15, 2019*. ACM, 499–513.
- [12] Yaohui Chen, Peng Li, Jun Xu, Shengjian Guo, Rundong Zhou, Yulong Zhang, Tao Wei, and Long Lu. 2020. SAVIOR: Towards Bug-Driven Hybrid Testing. In *2020 IEEE Symposium on Security and Privacy, SP 2020, San Francisco, CA, USA, May 18-21, 2020*. IEEE, 1580–1596. <https://doi.org/10.1109/SP40000.2020.00002>
- [13] Zhengjie Du, Yuekang Li, Yang Liu, and Bing Mao. 2022. WindRanger: A Directed Greybox Fuzzer driven by DeviationBasic Blocks. In *ICSE '22: 44st International Conference on Software Engineering*. ACM.
- [14] Shuitao Gan, Chao Zhang, Peng Chen, Bodong Zhao, Xiaojun Qin, Dong Wu, and Zuoning Chen. 2020. GREYONE: Data Flow Sensitive Fuzzing. In *29th USENIX Security Symposium (USENIX Security 20)*. USENIX Association, 2577–2594. <https://www.usenix.org/conference/usenixsecurity20/presentation/gan>
- [15] Vijay Ganesh, Tim Leek, and Martin Rinard. 2009. Taint-based directed whitebox fuzzing. In *2009 IEEE 31st International Conference on Software Engineering*. 474–484.
- [16] Heqing Huang, Yiyuan Guo, Qingkai Shi, Peisen Yao, Rongxin Wu, and Charles Zhang. 2022. Beacon: Directed Grey-Box Fuzzing with Provable Path Pruning. In *The 43rd IEEE Symposium on Security and Privacy(S&P'22)*.
- [17] Juhwan Kim and Joobeom Yun. 2019. Poster: Directed Hybrid Fuzzing on Binary Code. In *the 2019 ACM SIGSAC Conference*.
- [18] J. Kim and J. Yun. 2019. Poster: Directed Hybrid Fuzzing on Binary Code. In *the 2019 ACM SIGSAC Conference*.
- [19] Tor Lattimore. 2016. Regret Analysis of the Finite-Horizon Gittins Index Strategy for Multi-Armed Bandits. In *Proceedings of the 29th Conference on Learning Theory, COLT 2016, New York, USA, June 23-26, 2016 (JMLR Workshop and Conference Proceedings, Vol. 49)*, Vitaly Feldman, Alexander Rakhlin, and Ohad Shamir (Eds.). JMLR.org, 1214–1245. <http://proceedings.mlr.press/v49/lattimore16.html>
- [20] kcamtu. 2023. *American Fuzzy Lop (AFL) Fuzzer*.
- [21] Gwangmu Lee, Woohul Shim, and Byoungyoung Lee. 2021. Constraint-guided Directed Greybox Fuzzing. In *30th USENIX Security Symposium (USENIX Security 21)*. USENIX Association, 3559–3576. <https://www.usenix.org/conference/usenixsecurity21/presentation/lee-gwangmu>
- [22] Caroline Lemieux and Koushik Sen. 2018. FairFuzz: a targeted mutation strategy for increasing greybox fuzz testing coverage. In *Proceedings of the 33rd ACM/IEEE International Conference on Automated Software Engineering, ASE 2018, Montpellier, France, September 3-7, 2018*. ACM, 475–485. <https://doi.org/10.1145/3238147.3238176>
- [23] Yuwei Li, Shouling Ji, Yuan Chen, Sizhuang Liang, Wei-Han Lee, Yueyao Chen, Chenyang Lyu, Chunming Wu, Raheem Beyah, Peng Cheng, Kangjie Lu, and Ting Wang. 2021. UNIFUZZ: A Holistic and Pragmatic Metrics-Driven Platform for Evaluating Fuzzers. In *30th USENIX Security Symposium, USENIX Security 2021, August 11-13, 2021*. USENIX Association, 2777–2794. <https://www.usenix.org/conference/usenixsecurity21/presentation/li-yuwei>
- [24] Hongliang Liang, Lin Jiang, Lu Ai, and Jinyi Wei. 2020. Sequence Directed Hybrid Fuzzing. In *27th IEEE International Conference on Software Analysis, Evolution and Reengineering, SANER 2020, London, ON, Canada, February 18-21, 2020*. IEEE, 127–137. <https://doi.org/10.1109/SANER48275.2020.9054807>
- [25] Hongliang Liang, Lin Jiang, Lu Ai, and Jinyi Wei. 2020. Sequence Directed Hybrid Fuzzing. In *27th IEEE International Conference on Software Analysis, Evolution and Reengineering, SANER 2020, London, ON, Canada, February 18-21, 2020*. IEEE, 127–137. <https://doi.org/10.1109/SANER48275.2020.9054807>
- [26] Hongliang Liang, Yini Zhang, Yue Yu, Zhuosi Xie, and Lin Jiang. 2019. Sequence Coverage Directed Greybox Fuzzing (ICPC '19). IEEE Press. <https://doi.org/10.1109/ICPC.2019.00044>
- [27] Hongliang Liang, Yini Zhang, Yue Yu, Zhuosi Xie, and Lin Jiang. 2019. Sequence Coverage Directed Greybox Fuzzing. In *2019 IEEE/ACM 27th International Conference on Program Comprehension (ICPC)*. 249–259. <https://doi.org/10.1109/ICPC.2019.00044>
- [28] Kin Keung Ma, Yit Phang Khoo, Jeffrey S. Foster, and Michael Hicks. 2011. Directed symbolic execution. In *Static Analysis - 18th International Symposium, SAS 2011, Venice, Italy, September 14-16, 2011. Proceedings*.
- [29] Paul Dan Marinescu and Cristian Cadar. 2013. KATCH: high-coverage testing of software patches. In *Joint Meeting of the European Software Engineering Conference and the ACM SIGSOFT Symposium on the Foundations of Software Engineering, ESEC/FSE '13, Saint Petersburg, Russian Federation, August 18-26, 2013*. ACM, 235–245. <https://doi.org/10.1145/2491411.2491438>
- [30] Manh-Dung Nguyen, Sébastien Bardin, Richard Bonichon, Roland Groz, and Matthieu Lemerre. 2020. Binary-level Directed Fuzzing for Use-After-Free Vulnerabilities. In *23rd International Symposium on Research in Attacks, Intrusions and Defenses, RAID 2020, San Sebastian, Spain, October 14-15, 2020*. USENIX Association, 47–62. <https://www.usenix.org/conference/raid2020/presentation/nguyen>
- [31] Yannic Noller, Rody Kersten, and Corina S. Pasareanu. 2019. Badger: Complexity Analysis with Fuzzing and Symbolic Execution. In *Software Engineering and Software Management, SE/SWM 2019, Stuttgart, Germany, February 18-22, 2019 (LNI, Vol. P-292)*, Steffen Becker, Ivan Bogicevic, Georg Herzog, and Stefan Wagner (Eds.). GI, 65–66. <https://doi.org/10.18420/se2019-16>
- [32] Yannic Noller, Corina S. Pasareanu, Marcel Böhme, Youcheng Sun, Hoang Lam Nguyen, and Lars Grunske. 2020. HyDiff: hybrid differential software analysis. In *ICSE '20: 42nd International Conference on Software Engineering, Seoul, South Korea, 27 June - 19 July, 2020*, Gregg Rothermel and Doo-Hwan Bae (Eds.). ACM, 1273–1285. <https://doi.org/10.1145/3377811.3380363>
- [33] Jiaqi Peng, Feng Li, Bingchang Liu, Lili Xu, Binghong Liu, Kai Chen, and Wei Huo. 2019. 1dVul: Discovering 1-Day Vulnerabilities through Binary Patches. In *49th Annual IEEE/IFIP International Conference on Dependable Systems and Networks, DSN 2019, Portland, OR, USA, June 24-27, 2019*. IEEE, 605–616. <https://doi.org/10.1109/DSN.2019.00066>
- [34] Jiaqi Peng, Feng Li, Bingchang Liu, Lili Xu, Binghong Liu, Kai Chen, and Wei Huo. 2019. 1dVul: Discovering 1-Day Vulnerabilities through Binary Patches. In *49th Annual IEEE/IFIP International Conference on Dependable Systems and Networks, DSN 2019, Portland, OR, USA, June 24-27, 2019*. IEEE, 605–616. <https://doi.org/10.1109/DSN.2019.00066>

- //doi.org/10.1109/DSN.2019.00066
- [35] R. L. PLACKETT. 1958. STUDIES IN THE HISTORY OF PROBABILITY AND STATISTICS: VII. THE PRINCIPLE OF THE ARITHMETIC MEAN. *Biometrika* 45 (1958), 130–135. Issue 1-2. <https://doi.org/10.1093/biomet/45.1-2.130>
- [36] Sebastian Poeplau and Aurélien Francillon. 2020. Symbolic execution with SymCC: Don't interpret, compile!. In *29th USENIX Security Symposium, USENIX Security 2020, August 12-14, 2020*, Srdjan Capkun and Franziska Roesner (Eds.). USENIX Association, 181–198. <https://www.usenix.org/conference/usenixsecurity20/presentation/poeplau>
- [37] Konstantin Serebryany, Derek Bruening, Alexander Potapenko, and Dmitriy Vyukov. 2012. AddressSanitizer: A Fast Address Sanity Checker. In *2012 USENIX Annual Technical Conference (USENIX ATC 12)*. USENIX Association, Boston, MA, 309–318. <https://www.usenix.org/conference/atc12/technical-sessions/presentation/serebryany>
- [38] Abhishek Shah, Dongdong She, Samanway Sadhu, Krish Singal, Peter Coffman, and Suman Jana. 2022. MC2: Rigorous and Efficient Directed Greybox Fuzzing (CCS '22). Los Angeles, CA, USA. <https://doi.org/10.1145/3548606.3560648>
- [39] Y. Shin and L. Williams. 2013. Can traditional fault prediction models be used for vulnerability prediction? *Empirical Software Engineering* 18, 1 (2013), 25–59.
- [40] Haijun Wang, Xiaofei Xie, Yi Li, Cheng Wen, Yuekang Li, Yang Liu, Shengchao Qin, Hongxu Chen, and Yulei Sui. 2020. Typestate-guided fuzzer for discovering use-after-free vulnerabilities. In *ICSE '20: 42nd International Conference on Software Engineering, Seoul, South Korea, 27 June - 19 July, 2020*. ACM, 999–1010. <https://doi.org/10.1145/3377811.3380386>
- [41] Haijun Wang, Xiaofei Xie, Yi Li, Cheng Wen, Yuekang Li, Yang Liu, Shengchao Qin, Hongxu Chen, and Yulei Sui. 2020. Typestate-guided fuzzer for discovering use-after-free vulnerabilities. In *ICSE '20: 42nd International Conference on Software Engineering, Seoul, South Korea, 27 June - 19 July, 2020*. ACM, 999–1010. <https://doi.org/10.1145/3377811.3380386>
- [42] Xinyu Wang, Jun Sun, Zhenbang Chen, Peixin Zhang, Jingyi Wang, and Yun Lin. 2018. Towards optimal concolic testing. In *Proceedings of the 40th International Conference on Software Engineering, ICSE 2018, Gothenburg, Sweden, May 27 - June 03, 2018*. ACM, 291–302. <https://doi.org/10.1145/3180155.3180177>
- [43] Y. Wang, X. Jia, Y. Liu, K. Zeng, and P. Su. 2020. Not All Coverage Measurements Are Equal: Fuzzing by Coverage Accounting for Input Prioritization. In *Network and Distributed System Security Symposium*.
- [44] Cheng Wen, Haijun Wang, Yuekang Li, Shengchao Qin, Yang Liu, Zhiwu Xu, Hongxu Chen, Xiaofei Xie, Geguang Pu, and Ting Liu. 2020. MemLock: memory usage guided fuzzing. In *ICSE '20: 42nd International Conference on Software Engineering, Seoul, South Korea, 27 June - 19 July, 2020*. ACM, 765–777. <https://doi.org/10.1145/3377811.3380396>
- [45] Yang, Guowei, Rungta, Neha, Khurshid, Sarfraz, Person, and Suzette. 2011. Directed incremental symbolic execution. *ACM SIGPLAN Notices: A Monthly Publication of the Special Interest Group on Programming Languages* (2011).
- [46] Insu Yun, Sangho Lee, Meng Xu, Yeongjin Jang, and Taesoo Kim. 2018. QSYM : A Practical Concolic Execution Engine Tailored for Hybrid Fuzzing. In *27th USENIX Security Symposium, USENIX Security 2018, Baltimore, MD, USA, August 15-17, 2018*, William Enck and Adrienne Porter Felt (Eds.). USENIX Association, 745–761. <https://www.usenix.org/conference/usenixsecurity18/presentation/yun>
- [47] Lei Zhao, Yue Duan, Heng Yin, and Jifeng Xuan. 2019. Send Hardest Problems My Way: Probabilistic Path Prioritization for Hybrid Fuzzing. In *26th Annual Network and Distributed System Security Symposium, NDSS*

2019, San Diego, California, USA, February 24-27, 2019. The Internet Society. <https://www.ndss-symposium.org/ndss-paper/send-hardest-problems-my-way-probabilistic-path-prioritization-for-hybrid-fuzzing/>

[48] Peiyuan Zong, Tao Lv, Dawei Wang, Zizhuang Deng, Ruigang Liang, and Kai Chen. 2020. FuzzGuard: Filtering out Unreachable Inputs in Directed Grey-box Fuzzing through Deep Learning. In *29th USENIX Security Symposium (USENIX Security 20)*. USENIX Association, 2255–2269. <https://www.usenix.org/conference/usenixsecurity20/presentation/zong>

9 APPENDIX

Table 4: The programs tested for discovering new vulnerabilities

No	Prog	Version
1	cflow	1.6
2	mp42aac	Bento4 1.5.1-628
3	jhead	3.00
4	mp3gain	1.5.2
5	lame	3.99.5
6	imginfo	jasper 2.0.12
7	gdk-pixbuf-pixdata	gdk-pixbuf 2.31.1
8	jq	1.5
9	tcpdump	4.8.1
10	tic	ncurses 6.1
11	flvmeta	1.2.1
12	tiffsplit	libtiff 3.9.7
13	nm	binutils-5279478
14	pdftotext	4.00
15	sqlite3	SQLite 3.8.9
16	exiv2	0.26
17	fig2dev	3.2.7a
18	gifsicle	1.90
19	jbig2dec	0.16
20	freetype	2.10.0
21	ImageMagick	7.0.8.6
22	libjpeg-turbo	1.5.1
23	libpng	1.6.37
24	pdftops	Libpoppler 0.74
25	GraphicsM	1.3.28

Table 5: The TTR results on programs from UniBench

No	Prog	Version	Target sites	AFLGo	AFLSy	BEACON	Wind	Parne	HyperGo
1	cflow	1.6	parser.c:281	T.O.	T.O.	99.4m	61.1m	T.O.	51.8m
2			c.c:1783	12.8m	9.43m	22.1m	6.45m	10.1m	8.82m
3			parser.c:105	0.82m	1.21m	13.5m	0.93m	0.44m	1.68m
4			parser.c:1223	1.22m	1.66m	0.83m	2.44m	6.23m	10.8m
5			parser.c:108	12.8m	8.63m	68.1m	8.32m	6.76m	1.65m
6	mp42aac	Bento4 1.5.1-628	Ap4AvccAtom.cpp:82	T.O.	T.O.	N/A	T.O.	N/A	1124m
7			Ap4TrunAtom.cpp:139	T.O.	T.O.	N/A	T.O.	N/A	223m
8			Ap4SbpgAtom.cpp:81	T.O.	T.O.	N/A	T.O.	N/A	781m
9			Ap4TfdtAtom.cpp:71	T.O.	985m	N/A	T.O.	N/A	166m
10			Ap4AtomFactory.cpp:490	T.O.	1324m	N/A	T.O.	N/A	215m
11	jhead	3.00	exif.c:1339	T.O.	T.O.	N/A	T.O.	T.O.	5.52m
12			exif.c:1327	T.O.	T.O.	N/A	T.O.	T.O.	2.74m
13			iptc.c:143	T.O.	T.O.	N/A	T.O.	T.O.	107m
14			iptc.c:91	T.O.	T.O.	N/A	T.O.	T.O.	20.8m
15			makernote.c:174	T.O.	1102m	N/A	T.O.	T.O.	11.3m
16	mp3gain	1.5.2	layer3.c:1116	1142m	841m	N/A	984m	N/A	10.84m
17			interface.c:690	1098m	81.9m	N/A	324m	N/A	9.02m
18			mp3gain.c:602	T.O.	T.O.	N/A	T.O.	N/A	119m
19			interface.c:663	T.O.	T.O.	N/A	T.O.	N/A	12.8m
20			apetag.c:341	290m	132m	N/A	91.2m	N/A	11.8m
21	lame	3.99.5	bitstream.c:823	T.O.	T.O.	N/A	T.O.	N/A	36.8m
22			lame.c:2148	T.O.	T.O.	N/A	T.O.	N/A	8.73m
23			uantize_pvt.c:441	T.O.	T.O.	N/A	1269m	N/A	354m
24			VbrTag.c:778	26.5 m	1.42m	N/A	39.1m	N/A	2.96m
25			get_audio.c:1605	T.O.	T.O.	N/A	T.O.	N/A	11.5m
26	imginfo	jasper 2.0.12	jp2_cod.c:841	T.O.	T.O.	N/A	T.O.	T.O.	451m
27			jpc_dec.c:1393	T.O.	89.1m	N/A	653m	T.O.	0.35m
28			jp2_cod.c:636	T.O.	T.O.	N/A	T.O.	T.O.	314m
29			jas_stream.c:823	T.O.	1123m	N/A	T.O.	T.O.	0.71m
30			jpc_dec.c:1393	T.O.	121m	N/A	T.O.	984m	0.81m
31	gdk-pixbuf-pixdata	gdk-pixbuf 2.31.1	gdk-pixbuf-loader.c:387	T.O.	T.O.	T.O.	T.O.	N/A	1339m
32			io-qtif.c:511	T.O.	T.O.	T.O.	T.O.	N/A	841m
33			io-ani.c:403	T.O.	T.O.	T.O.	T.O.	N/A	72.3m
34			io-jpeg.c:691	T.O.	T.O.	T.O.	T.O.	N/A	68.6m
35			io-tga.c:360	126m	111m	T.O.	T.O.	N/A	60.7m
36	jq	1.5	jv_dtoa.c:3122	T.O.	T.O.	T.O.	N/A	T.O.	1223m
37			jv_dtoa.c:2004	T.O.	T.O.	T.O.	N/A	T.O.	1163m
38			jv_dtoa.c:2518	T.O.	T.O.	T.O.	N/A	T.O.	875m
39			jv_unicode.c:42	T.O.	T.O.	T.O.	N/A	T.O.	864m
40			jv_dtoa.c:3044	T.O.	T.O.	T.O.	N/A	T.O.	37.1m
41	tcpdump	4.8.1	print-aodv.c:259	T.O.	T.O.	N/A	843m	T.O.	124m
42			print-ntp.c:412	1436m	1311m	N/A	974m	1239m	33.7m
43			print-rsvp.c:1252	T.O.	T.O.	N/A	T.O.	889m	194m
44			print-snmp.c:607	359m	412m	N/A	192m	992m	11.2m
45			print-l2tp.c:606	T.O.	T.O.	N/A	T.O.	T.O.	526m
46	tic	ncurses 6.1	captoinfo.c:189	T.O.	T.O.	N/A	N/A	T.O.	15.1m
47			alloc_entry.c:141	T.O.	T.O.	N/A	N/A	T.O.	19.1m
48			name_match.c:111	1186m	866m	N/A	N/A	T.O.	19.5m
49			comp_scan.c:860	264m	49.3m	N/A	N/A	168m	1.10m
50			entries.c:78	1038m	1134m	N/A	N/A	883m	19.9m
51	flvmeta	1.2.1	json.c:1036	T.O.	T.O.	N/A	T.O.	T.O.	10.1m
52			avc.c:1023	T.O.	T.O.	N/A	T.O.	T.O.	12.9m
53			api.c:718	T.O.	T.O.	N/A	T.O.	T.O.	50.1m
54			flvmeta.c:1023	T.O.	T.O.	N/A	T.O.	T.O.	60.6m
55			check.c:769	T.O.	T.O.	N/A	T.O.	T.O.	74.7m
56	tiffsplit	libtiff 3.9.7	tif_ojpeg.c:1277	T.O.	188m	N/A	T.O.	N/A	7.41m
57			tif_read.c:335	T.O.	T.O.	N/A	T.O.	N/A	1321m
58			tif_jbig.c:277	T.O.	T.O.	N/A	T.O.	N/A	967m
59			tif_dirread.c:1977	T.O.	T.O.	N/A	T.O.	N/A	388m
60			tif_strip.c:154	1328m	1139m	N/A	T.O.	N/A	8.73m
61	nm	binutils-5279478	tekhex.c:325	T.O.	T.O.	364m	798m	N/A	78.4m
62			elf.c:8793	T.O.	T.O.	986m	T.O.	N/A	102m
63			dwarf2.c:2378	1313m	868m	831m	1065m	N/A	357m
64			dwarf1.c:281	T.O.	268m	98m	T.O.	N/A	187m
65			elf-properties.c:51	T.O.	T.O.	T.O.	T.O.	N/A	853m
66	pdftotext	4.00	XRef.cc:645	T.O.	T.O.	N/A	T.O.	N/A	201m
67			Stream.cc:2658	T.O.	T.O.	N/A	T.O.	N/A	201m
68			GfxFont.cc:1337	1345m	1223m	N/A	T.O.	N/A	17.5m
69			Stream.cc:1004	725m	824m	N/A	T.O.	N/A	207m
70			GfxFont.cc:1643	637m	514m	N/A	T.O.	N/A	1004m
71	sqlite3	SQLite 3.8.9	pager.c:5017	617m	436m	N/A	N/A	1214m	44.1m
72			select.c:4301	T.O.	T.O.	367m	N/A	T.O.	2.55m
73			func.c:1029	T.O.	T.O.	T.O.	N/A	T.O.	896m
74			insert.c:1498	T.O.	T.O.	T.O.	N/A	T.O.	857m
75			vdbe.c:1984	T.O.	T.O.	89.6m	N/A	T.O.	0.90m
76	exiv2	0.26	tiffcomposite.cpp:82	73.1m	59.3m	N/A	68.1m	N/A	1.90m
77			XMPMeta-Parse.cpp:1037	126m	78.1m	N/A	168m	N/A	21.8m
78			XMPMeta-Parse.cpp:847	37.5m	13.4m	N/A	21.4m	N/A	39.8m
79			tiffvisitor.cpp:1044	102m	111m	N/A	T.O.	N/A	39.5m
80			XMPMeta-Parse.cpp:896	86.7m	78.4m	N/A	421m	N/A	1.72m
speedup				38.74×	30.89×	28.52×	106×	143×	-
mean A_{12}				0.88	0.85	0.92	0.86	0.91	-
mean p-values				0.002	0.008	0.008	0.003	0.001	-

Table 6: The TTR results of the incremental experiments on programs from UniBench

No	Prog	Version	Target sites	AFLGoSy	Only-PB	PB+DMAB	HyperGo
1			parser.c:281	T.O.	311m	224m	51.8m
2			c.c:1783	9.43m	8.41m	7.09m	8.82m
3	cflow	1.6	parser.c:105	1.21m	2.37m	2.88m	1.68m
4			parser.c:1223	1.66m	2.44m	7.21m	10.8m
5			parser.c:108	8.63m	4.33m	2.69m	1.65m
6			Ap4AvccAtom.cpp:82	T.O.	T.O.	T.O.	1124m
7			Ap4TrunAtom.cpp:139	T.O.	T.O.	T.O.	223m
8	mp42aac	Bento4 1.5.1-628	Ap4SbgpAtom.cpp:81	T.O.	T.O.	T.O.	781m
9			Ap4TfdtAtom.cpp:71	985m	304m	287m	166m
10			Ap4AtomFactory.cpp:490	1324m	1318m	1311m	215m
11			exif.c:1339	T.O.	T.O.	T.O.	5.52m
12			exif.c:1327	T.O.	T.O.	T.O.	2.7m
13	jhead	3.00	iptc.c:143	T.O.	T.O.	T.O.	107m
14			iptc.c:91	T.O.	T.O.	771m	20.8m
15			makernote.c:174	1102m	417m	349m	11.3m
16			layer3.c:1116	841m	262m	229m	10.8m
17			interface.c:690	81.9m	67.6m	61.1	9.02m
18	mp3gain	1.5.2	mp3gain.c:602	T.O.	T.O.	771m	119m
19			interface.c:663	T.O.	T.O.	T.O.	12.8m
20			apetag.c:341	132m	132m	67.4m	11.8m
21			bitstream.c:823	T.O.	761m	627m	36.8m
22			lame.c:2148	T.O.	T.O.	T.O.	8.7m
23	lame	3.99.5	uantize_pvt.c:441	T.O.	T.O.	T.O.	354m
24			VbrTag.c:778	1.42m	1.40m	1.41m	2.96m
25			get_audio.c:1605	T.O.	T.O.	T.O.	11.5m
26			jp2_cod.c:841	T.O.	T.O.	T.O.	451m
27			jpc_dec.c:1393	89.1m	39.0m	33.1m	0.35m
28	imginfo	jasper 2.0.12	jp2_cod.c:636	T.O.	T.O.	T.O.	314m
29			jas_stream.c:823	1123m	1101m	1088m	0.71m
30			jpc_dec.c:1393	121m	26.8m	23.0m	0.81m
31			gdk-pixbuf-loader.c:387	T.O.	T.O.	T.O.	1339m
32			io-qtif.c:511	T.O.	T.O.	T.O.	841m
33	gdk-pixbuf-pixdata	gdk-pixbuf 2.31.1	io-ani.c:403	T.O.	T.O.	T.O.	72.3m
34			io-jpeg.c:691	T.O.	T.O.	T.O.	68.6m
35			io-tga.c:360	111m	106m	74.1m	60.7m
36			jv_dtoa.c:3122	T.O.	T.O.	1241m	1223m
37			jv_dtoa.c:2004	T.O.	T.O.	T.O.	1163m
38	jq	1.5	jv_dtoa.c:2518	T.O.	T.O.	T.O.	875m
39			jv_unicode.c:42	T.O.	T.O.	T.O.	864m
40			jv_dtoa.c:3044	T.O.	T.O.	929m	37.1m
41			print-aodv.c:259	T.O.	T.O.	T.O.	124m
42			print-ntp.c:412	1311m	801m	383m	33.7m
43	tcpdump	4.8.1	print-rsvp.c:1252	T.O.	T.O.	T.O.	194m
44			print-snmp.c:607	412m	124m	992m	11.2m
45			print-l2tp.c:606	T.O.	T.O.	T.O.	526m
46			captinfo.c:189	T.O.	T.O.	T.O.	15.1m
47			alloc_entry.c:141	T.O.	T.O.	T.O.	19.1m
48	tic	ncurses 6.1	name_match.c:111	866m	623m	86.6m	19.5m
49			comp_scan.c:860	49.3m	14.3m	7.24m	1.10m
50			entries.c:78	1134m	824m	336m	19.9m
51			json.c:1036	T.O.	T.O.	T.O.	10.1m
52			avc.c:1023	T.O.	T.O.	T.O.	12.9m
53	flvmeta	1.2.1	api.c:718	T.O.	T.O.	T.O.	50.1m
54			flvmeta.c:1023	T.O.	T.O.	T.O.	60.6m
55			check.c:769	T.O.	T.O.	T.O.	74.7m
56			tif_ojpeg.c:1277	188.4m	79.7m	60.4m	7.41m
57			tif_read.c:335	T.O.	T.O.	T.O.	1321m
58	tiffsplit	libtiff 3.9.7	tif_jbig.c:277	T.O.	T.O.	T.O.	967m
59			tif_dirread.c:1977	T.O.	T.O.	T.O.	388m
60			tif_strip.c:154	1139m	926m	796m	8.73m
61			tekhex.c:325	T.O.	T.O.	T.O.	78.4m
62			elf.c:8793	T.O.	T.O.	T.O.	102m
63	nm	binutils-5279478	dwarf2.c:2378	868m	553m	512m	357m
64			dwarf1.c:281	268m	241m	233m	187m
65			elf-properties.c:51	T.O.	T.O.	T.O.	853m
66			XRef.c:645	T.O.	T.O.	T.O.	201m
67			Stream.cc:2658	T.O.	T.O.	T.O.	201m
68	pdfotext	4.00	GfxFont.cc:1337	1223m	1208m	579m	17.5m
69			Stream.cc:1004	824m	631m	330m	207m
70			GfxFont.cc:1643	514m	477m	586m	1004m
71			pager.c:5017	436m	196m	174m	44.1m
72			select.c:4301	T.O.	T.O.	T.O.	2.55m
73	sqlite3	SQLite 3.8.9	func.c:1029	T.O.	T.O.	T.O.	896m
74			insert.c:1498	T.O.	T.O.	T.O.	857m
75			vdbe.c:1984	T.O.	T.O.	T.O.	0.90m
76			tiffcomposite.cpp:82	59.3m	26.0m	27.6m	1.90m
77			XMPMeta-Parse.cpp:1037	78.1m	72.9m	60.5m	21.8m
78	exiv2	0.26	XMPMeta-Parse.cpp:847	13.4m	16.2m	14.3m	39.8m
79			tiffvisitor.cpp:1044	111m	109m	93.8m	39.5m
80			XMPMeta-Parse.cpp:896	78.4m	95.3m	57.2m	1.72m
speedup				-	1.33×	1.84×	30.89×
mean \hat{A}_{12}				-	0.73	0.79	0.85
mean p-values				-	0.024	0.018	0.008